Original Article

MOLECULAR METABOLISM

The conserved Mediator subunit cyclin C (CCNC) is required for brown adipocyte development and lipid accumulation

Ziyi Song [1,2,3,5], Alus M. Xiaoli [2,3,5,], Youlei Li [2,3,5], Gerile Siqin [2,3,5], Tian Wu [1], Randy Strich [6], Jeffrey E. Pessin [2,4,5], Fajun Yang [2,3,5,*]**

ABSTRACT

Objective: Cyclin C (CCNC) is the most conserved subunit of the Mediator complex, which is an important transcription cofactor. Recently, we have found that CCNC facilitates brown adipogenesis *in vitro* by activating C/EBPα-dependent transcription. However, the role of CCNC in brown adipose tissue (BAT) *in vivo* remains unclear.

Methods: We generated conditional knock-out mice by crossing *Ccnc*$^{flox/flox}$ mice with *Myf5*^{Cre}, *Ucp1*^{Cre} or *Adipoq*^{Cre} transgenic mice to investigate the role of CCNC in BAT development and function. We applied glucose and insulin tolerance test, cold exposure and indirect calorimetry to capture the physiological phenotypes and used immunostaining, immunoblotting, qRT-PCR, RNA-seq and cell culture to elucidate the underlying mechanisms.

Results: Here, we show that deletion of CCNC in *Myf5*$^{+}$ progenitor cells caused BAT paucity, despite the fact that there was significant neonatal lethality. Mechanistically different from *in vitro*, CCNC deficiency impaired the proliferation of embryonic brown fat progenitor cells without affecting brown adipogenesis or cell death. Interestingly, CCNC deficiency robustly reduced age-dependent lipid accumulation in differentiated brown adipocytes in all three mouse models. Mechanistically, CCNC in brown adipocytes is required for lipogenic gene expression through the activation of the C/EBPα/GLUT4/ChREBP axis. Consistent with the importance of *de novo* lipogenesis under carbohydrate-rich diets, high-fat diet (HFD) feeding abolished CCNC deficiency -caused defects of lipid accumulation in BAT. Although insulin sensitivity and response to acute cold exposure were not affected, CCNC deficiency in *Ucp1*$^{+}$ cells enhanced the browning of white adipose tissue (beiging) upon prolonged cold exposure.

Conclusions: Together, these data indicate an important role of CCNC-Mediator in the regulation of BAT development and lipid accumulation in brown adipocytes.

Keywords CCNC; brown fat; Lipid droplet; Progenitor; Proliferation; Lipogenesis

1. INTRODUCTION

The current epidemic of obesity and type 2 diabetes has increased the need for novel approaches to reduce adiposity. Obesity is caused by prolonged periods of positive energy balance in which energy intake exceeds energy expenditure. Brown adipose tissue (BAT) is specialized to dissipate energy through uncoupling protein 1 (UCP1) and thus may counteract obesity [1]. Rodents also displays an inducible thermogenic adipose tissue termed beige adipocytes that arises within white adipose tissue (WAT) depots, that can use both UCP1 and possibly other futile cycles for heat production [2,3]. In humans, BAT is abundant at birth but is rapidly replaced by WAT through unknown mechanisms and is relatively scarce in adults as an unidentifiable tissue [4]. However, studies with ^{18}fluoro-labelled 2-deoxy-glucose positron emission tomography (^{18}FDG-PET) scanning demonstrated that adult humans could have active thermogenic adipose tissue deposits and the amount of this thermogenic tissue is inversely correlated with adiposity and body mass index (BMI) [5,6]. Whether human

[1]State Key Laboratory for Conservation and Utilization of Subtropical Agro-bioresources, College of Animal Science and Technology, Guangxi University, Nanning, 530004, China [2]Department of Medicine, Albert Einstein College of Medicine, Bronx, NY, 10461, USA [3]Department of Developmental and Molecular Biology, Albert Einstein College of Medicine, Bronx, NY, 10461, USA [4]Department of Molecular Pharmacology, Albert Einstein College of Medicine, Bronx, NY, 10461, USA [5]Department of Norman Fleischer Institute for Diabetes and Metabolism, Albert Einstein College of Medicine, Bronx, NY, 10461, USA [6]Department of Molecular Biology, Rowan University School of Osteopathic Medicine, Stratford, NJ, 08055, USA

*Corresponding author. Albert Einstein College of Medicine, Departments of Medicine, and Developmental and Molecular Biology, 1301 Morris Park Avenue, Price Center, Room 377, Bronx, NY, 10461, USA. Fax: +1 718 678 1020. E-mail: fajun.yang@einsteinmed.edu (F. Yang).

**Corresponding author. E-mail: alus.xiaoli@einsteinmed.edu (A.M. Xiaoli).

Abbreviations: CCNC, cyclin C; BAT, brown adipose tissue; UCP1, uncoupling protein 1; C/EBP, CCAAT/enhancer-binding protein; ChREBP, carbohydrate response element-binding protein; SREBP, sterol regulatory element-binding protein

Received June 3, 2022 • Revision received July 5, 2022 • Accepted July 11, 2022 • Available online 19 July 2022

https://doi.org/10.1016/j.molmet.2022.101548

thermogenic adipose tissues are more reflective of rodent brown or beige adipocytes has not been fully resolved. In any case, activation of BAT thermogenesis by cold exposure, or by β3-adrenergic receptor agonist, has been linked to increased energy expenditure, reduced adiposity and lower plasma lipids [7–9], indicating that BAT plays an important role in energy homeostasis both in animal models and humans. Therefore, a better understanding of the molecular control of BAT development and function may lead to new therapeutic avenues to combat obesity and metabolic disorders.

The classical brown fat is localized in the interscapular region in rodents and arises from a *Myf5*-positive lineage [10]. PR-domain-containing protein 16 (PRDM16), a BAT-enriched transcription cofactor, acts as a fate switch to control brown adipocyte versus myocyte between days 9–12 of gestation in mice [10,11]. Mechanistically, PRDM16 forms a transcriptional complex with the active form of CCAAT/enhancer-binding protein-beta (C/EBPβ) in the myogenic precursors to activate the brown adipogenic gene program by inducing peroxisome proliferator-activated receptor-gamma (PPARγ) expression [12]. Meanwhile, it has been shown that euchromatic histone-lysine N-methyltransferase 1 (EHMT1) is a BAT-enriched lysine methyltransferase in complex with PRDM16 and regulates brown adipocyte fate by stabilizing PRDM16 proteins [13]. Extracellularly, BMP7 signaling promotes brown adipocyte differentiation and thermogenesis through the induction of PRDM16 and PPARγ coactivator-1a (PGC-1a), which increase the expression of the brown fat marker UCP1 and adipogenic transcription factors PPARγ and C/EBPs as well as mitochondria biogenesis [14]. However, the regulatory mechanisms for BAT development are not completely understood.

Unlike white adipocytes, differentiated brown adipocytes are characterized by multilocular lipid droplets, in which triglycerides are increasingly accumulated with age. Although the physiological functions remain less clear, lipolysis and lipogenesis in BAT are dynamic and highly active in response to environmental cues. The regulation of lipolysis in BAT has been well documented [15,16], but the regulation of lipogenesis and triglyceride biosynthesis in BAT is less studied. Recently, one study has shown that AKT2, a cold-induced kinase, promotes *de novo* lipogenesis (DNL) in BAT through carbohydrate response element-binding protein (ChREBP) but not sterol regulatory element-binding protein-1 (SREBP-1) [17]. Moreover, DNL in BAT may play a role in optimizing fuel storage and thermogenesis in mice, as inhibition of DNL in BAT causes compensatory increase of WAT browning under prolonged cold exposure [17]. Importantly, brown fat DNL in human is positively correlated with *Ucp1* expression, and negatively correlated with BMI [17,18]. Although there have been significant insights into the signaling pathways and transcription factors that regulate DNL in BAT, the regulation of lipid metabolism in BAT remains largely unclear.

The Mediator complex is a conserved transcription cofactor that primarily regulates activator-dependent transcription [19–22]. In mammalian cells, the Mediator complex is comprised of up to 30 subunits [19–22]. It has been shown that the Mediator subunit MED1 regulates white adipogenesis *in vitro* through PPARγ [23,24]. MED14 [25], MED19 [26], MED23 [27,28] and MED31 [29] are also involved in the regulation of white adipogenesis *in vitro* and in mouse models through PPARγ and/or other aspects of insulin signaling pathway. Moreover, MED1 regulates the brown adipocyte transcriptional program by interacting with PRDM16 [30,31]. More recently, using tissue specific MED1 knockout mouse models, two studies have demonstrated a critical role of MED1 in adipose tissue formation *in vivo* [32,33]. On the other hand, the Mediator subunits MED1 [33], MED15 [34] and MED17 [35,36] are directly or indirectly involved in the induction of lipogenesis. Previously, we have shown that the Mediator subunit CDK8 together with its activating partner CCNC negatively regulates DNL in hepatocytes and *Drosophila* fat bodies by promoting nuclear SREBP-1a/c phosphorylation and subsequent degradation [37]. Although initially identified as a potential cell cycle regulator [38,39], CCNC functions to regulate gene transcription in the context of the Mediator complex. As a highly conserved Mediator subunit, CCNC has been shown to play multiple roles in various biological processes including cell proliferation [38–40], cell apoptosis [41,42], and cellular lipid metabolism [37,43]. Recently, we have identified CCNC as an essential regulator for brown adipogenesis *in vitro* [43]. Mechanistically, CCNC-Mediator physically interacts with C/EBPα and activates the C/EBPα transactivation domain activity to facilitate brown preadipocyte differentiation [43]. Interestingly, the CCNC level is decreased during brown adipogenesis and during aging in mice [43], suggesting that CCNC may play a role in BAT development and function. Human individuals with mutations in the genomic locus of *Cdk8*, one major effector of CCNC, are prone to develop type 2 diabetes [44]. Moreover, the GWAS Central data indicate that human *Ccnc* gene is significantly associated with BMI. However, the underlying mechanism remains unknown. Based on these findings, we hypothesize that CCNC plays an important role in BAT development and function *in vivo*. Here, we show that CCNC deletion in $Myf5^{+}$ cells caused a partial neonatal lethality in mice likely due to the developmental defects in rib cartilage. The survived CCNC-deficient mice displayed a paucity in BAT due to the impaired proliferation of brown adipocyte progenitor cells. In contrast to tissue culture, CCNC deficiency did not affect brown adipogenesis *in vivo*. Interestingly, CCNC-deficient BAT displayed a reduced ability of accumulating lipids over time when mice were fed with a carbohydrate-rich normal chow diet. This phenotype was recapitulated when CCNC was deleted in either $Ucp1^{+}$ or $Adipoq^{+}$ cells. RNA-seq analyses revealed that CCNC deficiency reduced the expression of some key enzymes for fatty acid and triglyceride biosynthesis that are critically regulated by the C/EBPα/GLUT4/ChREBP pathway. Consistent with the regulation of DNL, CCNC depletion -caused lipid accumulation defects in BAT was abolished when mice were fed with a high fat diet (HFD). Moreover, deletion of CCNC in $Ucp1^{+}$ cells also enhanced WAT beiging upon chronic cold exposure. Thus, our results indicate that CCNC plays a pivotal role in BAT prenatal development and postnatal lipid metabolism.

2. MATERIALS AND METHODS

2.1. Animals and diets

All mouse experiments conformed to the protocols approved by the Animal Care and Use Committees of the Albert Einstein College of Medicine in accordance with the National Institutes of Health guidelines. $Myf5^{Cre}$ (Stock #010529), $Ucp1^{Cre}$ (Stock #024670) and $Adipoq^{Cre}$ (Stock #028020) transgenic mice were obtained from the Jackson Laboratory. *Ccnc*-floxed mice was generated and backcrossed for ten generations into the C57BL/6J strain. Mice were housed in a pathogen-free animal facility at 22 °C with a 12 h light/dark cycle (7:00 am - 7:00 pm) with free access to water and the normal chow diet (#5053, LabDiet; 13 kcal% fat and 62 kcal% carbohydrate) or the high-fat diet (no. D12492, Research Diets; 60 kcal% fat and 20 kcal% carbohydrate), which started at the age of six weeks.

2.2. Body composition and indirect calorimetry

Fat/lean mass was measured by quantitative nuclear magnetic resonance (NMR) noninvasive imaging (EchoMRI, TX). Metabolic measurement was performed using an Oxymax indirect calorimetry system

(Columbus Instruments, Columbus, OH). Mice were individually housed in metabolic chambers at 22 °C with a 12 h light/dark cycle and free access to food and water. After acclimation in metabolic chambers for 48 h, energy expenditure, oxygen consumption (VO_2), carbon dioxide production (VCO_2), and spontaneous locomotor activity were measured as previously described [45]. VO_2, VCO_2, and energy expenditure of each mouse were normalized by its lean mass.

2.3. Glucose and insulin tolerance test (GTT and ITT)

For GTT, mice were fasted for 14 h and then received an intraperitoneal injection of glucose (1 g/kg body weight). Two weeks later, ITT was performed by an intraperitoneal injection of insulin (1.5 U/kg body weight) after 4 h fasting. Blood was collected at consecutive time points after the injection of glucose or insulin by tail bleeding, and blood glucose levels were measured using the AlphaTRAK 2 Blood Glucose Monitoring System.

2.4. Cold exposure

To assess cold tolerance, 8-month-old control and $Ccnc^{Ucp1(KO)}$ mice were fasted for 4 h in the morning, and then placed at 6 °C individually in pre-chilled cages with free access to pre-chilled water and food. Intrarectal temperatures were monitored and recorded with a TH-8 Thermalert Monitoring Thermometer (Physitemp Instruments, Clifton, NJ) at consecutive time points up to 14 days.

2.5. Measurement of triglycerides

Triglycerides in BAT were measured using the Triglyceride Quantification Colorimetric Fluorometric Kit (Biovision, Milpitas, CA) according to the manufacturer's instructions. Briefly, total lipids were extracted from homogenized BAT (~20 mg each), and triglycerides were converted to free fatty acids and glycerol by the addition of lipases. Glycerol was detected by an enzyme-coupled reaction and using a VersaMax spectrometry microplate reader (Molecular Devices, Sunnyvale, CA). The triglyceride levels were normalized by genomic DNA.

2.6. Alcian Blue-Alizarin Red staining

Dead $Ccnc^{Myf5(KO)}$ newborns and littermate controls (alive) were fixed in 4% paraformaldehyde for Alcian Blue-Alizarin Red staining as previously described with minor modifications [46]. Briefly, skins and tissues were carefully removed, and fat was depleted by washing with 95% ethanol followed by overnight incubation in acetone. The skeletons were immersed in 0.03% alcian blue solution for 24 h to stain cartilage, washed with 70% ethanol, and incubated in 1% potassium hydroxide until clear. Bone was counterstained with 0.03% alizarin red solution until sharply delineated. The stained samples were cleaned in 1% potassium hydroxide/glycerol (1:1) for a week and kept in glycerol at the end. Images were captured by a Nikon Digital Camera and processed using the Photoshop CS6 software.

2.7. TUNEL assay, immunofluorescence, immunohistochemistry and histological analyses

An 8-μm thick, 4% neutral buffered paraformaldehyde-fixed cryosections of tissues were embedded in an optimal cutting temperature compound. TUNEL assay was performed using the ApopTag Red in situ Apoptosis Detection Kit (EMD Millipore, Burlington, MA) according to the manufacturer's instructions. Briefly, sections were treated with the Equilibration Buffer and the Working Strength TdT Enzyme sequentially, and counterstained with an anti-digoxigenin conjugate antibody and mounted with the prolong antifade reagent with DAPI (Invitrogen) before imaging. For Ki67 immunofluorescent staining, slides were permeabilized with 0.3% Triton X-100 (Sigma—Aldrich), washed with 1xPBS, and blocked with 5% normal donkey serum (ab166643, Abcam) before adding anti-Ki67 primary antibody (ab16667, Abcam, 1:500) that was diluted in blocking solution. After wash, Alexa Flour 488-labelled secondary antibody (Invitrogen, 1:500) was added. The slides were then washed, counterstained, and mounted with the prolong antifade reagent with DAPI (Invitrogen) before imaging. For UCP1 immunohistochemical staining, 5 μm thick paraffin sections were deparaffinized, rehydrated, and epitopes unmasked by boiling with the Citra buffer (BioGenex, Fremont, CA). Tissues were then blocked with 5% normal goat serum solution before incubation with anti-UCP1 primary antibody (PA1-24894, Pierce, 1:200). Vectashield DAB Peroxidase Substrate Kit was used to detect the primary antibody. Sections were counterstained with hematoxylin, mounted, and imaged. For histological analyses, samples were embedded, cut, and performed Hematoxylin and Eosin (H&E) staining by the Albert Einstein College of Medicine Histology Core facility.

2.8. Western blotting

Cultured cells were washed with cold 1xPBS, scraped, and homogenized by pipetting in a lysis buffer containing 50 mM Tris—HCl (pH 8.0), 420 mM NaCl, 0.1 mM EDTA, 0.5% Nonidet P-40, 0.05% SDS, 10% Glycerol, and a Protease and Phosphatase Inhibitor Cocktail (78442, Thermo Fisher Scientific). Tissues were homogenized in the lysis buffer using Ceria Stabilized Zirconium Oxide Beads. The cell or tissue homogenates were centrifuged for 30 min at 21,000×*g* at 4 °C, and supernatants were collected for protein assays. Twenty μg of total proteins for each sample were loaded and separated by 4—12% SDS-PAGE and transferred to a nitrocellulose membrane using the iBlot Blotting System (Thermo Fisher Scientific). The membrane was blocked with 5% non-fat dry milk in 1x Tris-buffered saline containing Tween-20 (TBST) and incubated with a primary antibody in the blocking buffer. The membranes were washed with 1xTBST and incubated with HRP-conjugated secondary antibody in blocking buffer. The membrane was then washed with 1xTBST, visualized through ECL (Pierce, Thermo Fisher Scientific), and exposure to X-ray films. The following primary antibodies and dilutions were used: Anti-CCNC (558903,1:500) from BD Pharmingen; Anti-Actin (A5060, 1:200) from sigma; Anti-β-tubulin (1235662A, 1:2000) from Invitrogen; Anti-ChREBP (NBP2-44307, 1:500) from NOVUS; Anti-C/EBPa (8178, 1:250), Anti-FAS (3180, 1:1000) and Anti-ACC1 (3676, 1:1000) from Cell Signaling Technology; Anti-GLUT4 (ab654, 1:500) from Abcam; Anti-SREBP1 (sc-13551, 1:200) and Anti-CPT1B (sc-393070, 1:500) from Santa Cruz Biotechnology.

2.9. RNA extraction and real-time RT-PCR

Total RNA was prepared from tissue or cell samples using the Trizol Reagent (Invitrogen) according to the manufacturer's instructions. Genomic DNA contamination was removed by RNase-free DNase I (Thermo Scientific, USA). The quantity and quality of total RNA were determined by a spectrophotometer (Nanodrop 2000, Thermo Fisher). Total cDNA was synthesized from 1 μg of total RNA using iScript cDNA Synthesis Kit (BIO-RAD). Real-time PCR was performed using the PowerUp SYBR Green Master Mix (Thermo Fisher, USA). Specific primers for each gene are listed in Table S1. *Tbp* or *Rpl7* was used as the invariant control.

2.10. RNA sequencing (RNA-seq)

After RNA extraction from BAT of 6-month-old $Ccnc^{Ucp1(KO)}$ and control mice (three biological replicates each), RNA-seq libraries were prepared by the Einstein Genomics Core Facility. The library quality was analyzed by a Bioanalyzer (Agilent Technologies). Deep sequencing

was performed using a HiSeq 2500 instrument (Illumina). Raw reads for each library were mapped using TopHat version 2.0.8 against the indexed mouse (mm9) genome, and transcripts were assembled using Cufflinks. Genes that were not expressed in all samples (FPKM<1) were filtered out. Differentially expressed genes (DEGs) were identified using a RNA-seq processing tool DESeq2, selected by adjusted_p value < 0.05 and fold change >1.4 or < 0.5, and visualized using R tools ggplot2 and pheatmap, respectively. Kyoto encyclopedia of genes and genomes (KEGG) pathway enrichment analysis of DEGs was obtained from DAVID database (version 6.8). The heat map for the eight down-regulated genes in the insulin signaling pathway was based on the normalized reads, and they were listed according to their p values.

2.11. Tissue culture

Immortalized wildtype and CCNC-knockout brown preadipocytes were generated as shown previously [43]. These cells were maintained in DMEM with 25 mM glucose plus 10% FBS, 1% penicillin-streptomycin (P/S) and 1% L-glutamine. For differentiation, cells were cultured to confluent and then treated with the differentiation medium of DMEM containing dexamethasone (0.5 mM), insulin (20 nM), isobutylmethylxanthine (0.5 mM), indomethacin (0.125 mM), T3 (1 nM) and rosiglitozone (0.5 μM). After two days of culture, cells were maintained in DMEM containing 1 nM T3 and 20 nM insulin. Medium was replaced every other day. Full differentiation was achieved in about seven days.

2.12. Retrovirus transduction

Mouse ChREBPβ was amplified by PCR from pCMV-Flag-ChREBPα, which was a gift from Dr. Donald K. Scott of Icahn School of Medicine at Mount Sinai, and subcloned into the *EcoR*1 site of the retroviral vector pMSCV-PIG using an In-Fusion Cloning kit (Clontech) to generate a ChREBPβ-expressing plasmid, termed pMSCV-PIG-ChREBPβ, which was verified by DNA sequencing. Retroviral packaging plasmids, pUMVC (#8449) and pCMV-VSV-G (#8454), were obtained from Addgene. To generate pseudotyped virus, pUMVC, pCMV-VSV-G and pMSCV-PIG vectors were co-transfected into sub-confluent HEK293T cells using Lipofectamine 3000 Transfection Reagent (Invitrogen) according to the manufacturer's instructions. The virus stocks were collected at 48 h and 72 h after transfection, filtered through a 0.45 μm filter, and frozen at −80 °C. Brown preadipocytes (20−30% confluent) were infected with retrovirus stocks containing 8 μg/ml polybrene for 12 h, washed and cultured in DMEM.

2.13. Luciferase reporter assays

The constructs pcDNA3-Flag-C/EBPα (#66978) and 3xPPRE-TK-luc (#1015) were obtained from Addgene. The *Slc2a4* promoter was amplified from mouse genomic DNA by PCR [47], and subcloned into 3xPPRE-TK-luc by replacing the 3xPPRE sequence, which is located between *Hind III* and *BamH I* sites, using In-Fusion Cloning kit (Clontech). The resulting plasmid, *Slc2a4*-TK-luc, was verified by DNA sequencing. DNA transfection and luciferase reporter assays were conducted as described previously [43]. Briefly, brown preadipocytes were seeded at a density of 1×10^5 per well in 24-well plates. Next day, cells were transfected with a mix of 250 ng of pcDNA3-Flag-C/EBPα (or control), 250 ng of *Slc2a4*-TK-luc and 50 ng of renilla luciferase reporter using the Lipofectamine 3000 Transfection Reagent. After incubation for two days, cells were lysed and analyzed using the Dual-Luciferase System (Promega) according to the manufacturer's instructions. The firefly luciferase activity was normalized by the corresponding renilla luciferase activity.

2.14. Statistical analyses

All numerical results were expressed as Mean ± SD. Statistical difference was determined by unpaired Student's t-test at a significance level of $p < 0.05$. The statistical analyses and figure preparation were performed using GraphPad Prism 9 (GraphPad software).

3. RESULTS

3.1. CCNC deficiency in the *Myf5*$^+$ lineage causes partial neonatal lethality and reduction of brown adipose tissues

To understand the role of CCNC in BAT development, we deleted CCNC in *Myf5*$^+$ cells by crossing *Ccnc*$^{flox/flox}$ mice with *Myf5*^{Cre} transgenic mice, as *Myf5* is expressed specifically in the progenitor cells that give rise to brown adipocytes and skeletal muscle cells [10]. As shown in Figure 1A, genotyping analyses revealed that approximately 10% of mice were homozygous CCNC knockout (*Ccnc*$^{Myf5(KO)}$: *Ccnc*$^{flox/flox}$; *Myf5*^{Cre}) at the time of weaning. While the distribution of CCNC heterozygous or wildtype mice was closer to the expected 25% Mendelian ratio, the percentage of *Ccnc*$^{Myf5(KO)}$ mice was significantly lower than 25%, suggesting that many *Ccnc*$^{Myf5(KO)}$ mice may have died before weaning. Although a previous study has shown that germline CCNC ablation causes embryonic lethality at E10.5 [40], partial lethality of *Ccnc*$^{Myf5(KO)}$ pups was not expected. After closely monitoring the breeding pairs, we discovered an unusual number of dead newborns, and genotyping analyses showed that the majority of those dead pups (25 out of 30) were *Ccnc*$^{Myf5(KO)}$. However, genotyping analyses of embryos showed normal Mendelian ratios for all genotypes (Figure 1A), suggesting that the death of those *Ccnc*$^{Myf5(KO)}$ mice may have occurred shortly after birth.

It is unclear why CCNC deletion in *Myf5*$^+$ cells caused death in most but not all newborns. One possibility is hypothermia, because brown fat and skeletal muscle are important in the maintenance of body temperature in rodents [48]. Based on the *in vitro* data [43], we hypothesized that CCNC is required for BAT development *in vivo*. Thus, hypothermia could occur if BAT mass is less than normal. However, housing breeders at thermoneutrality (30 °C) did not improve the percentage of survived *Ccnc*$^{Myf5(KO)}$ mice (data not shown). Alternatively, another possibility is defects in rib structure or function that may be also dependent on *Myf5*$^+$ cells during the development [49—51]. To test this possibility, we examined the skeletons of dead *Ccnc*$^{Myf5(KO)}$ by Alcian Blue/Alizarin Red staining. As shown in Figure 1B, the ribs of dead *Ccnc*$^{Myf5(KO)}$ pups were obviously shorter and more fragile than those of control mice (*Ccnc*$^{flox/flox}$), suggesting that CCNC is also required for the rib cartilage development. Thus, it is likely that death of *Ccnc*$^{Myf5(KO)}$ newborns was due to respiratory failure.

Nevertheless, it was apparent that the survived *Ccnc*$^{Myf5(KO)}$ newborns had less interscapular BAT than control by size (Figure 1C—E). BAT from *Ccnc*$^{Myf5(KO)}$ mice weighed approximately 30% less than that of control (Figure 1F). However, the surviving *Ccnc*$^{Myf5(KO)}$ and control mice displayed similar in body weight (Figure 1G). In addition to genotyping, CCNC depletion in BAT of *Ccnc*$^{Myf5(KO)}$ mice at the mRNA level was verified by qRT-PCR (Figure 1H), and CCNC knockout did not affect the expression of its direct binding partners CDK8 or CDK19 (Figure 1H). Thus, despite the unexpected partial lethality, these results indicate that CCNC is important for the development of BAT.

3.2. CCNC is required for brown fat progenitor cell proliferation

Next, we sought to understand how CCNC deficiency in *Myf5*$^+$ cells could impair BAT development. There are three major possibilities that can cause the reduction of BAT: 1) reduced number of brown fat

A

Genotype	Embryos (E18.5) alive (%)	Newborns (P1) alive (%)	Expected rate (%)
Ccnc$^{flox/+}$	12 (22.2)	79 (31.5)	25.0
Ccnc$^{flox/flox}$ [Control]	14 (25.9)	90 (35.9)	25.0
Ccnc$^{flox/+}$; *Myf5*^{Cre}	14 (25.9)	58 (23.1)	25.0
Ccnc$^{flox/flox}$; *Myf5*^{Cre} [*Ccnc*$^{Myf5(KO)}$]	14 (25.9)	24 (9.56)	25.0

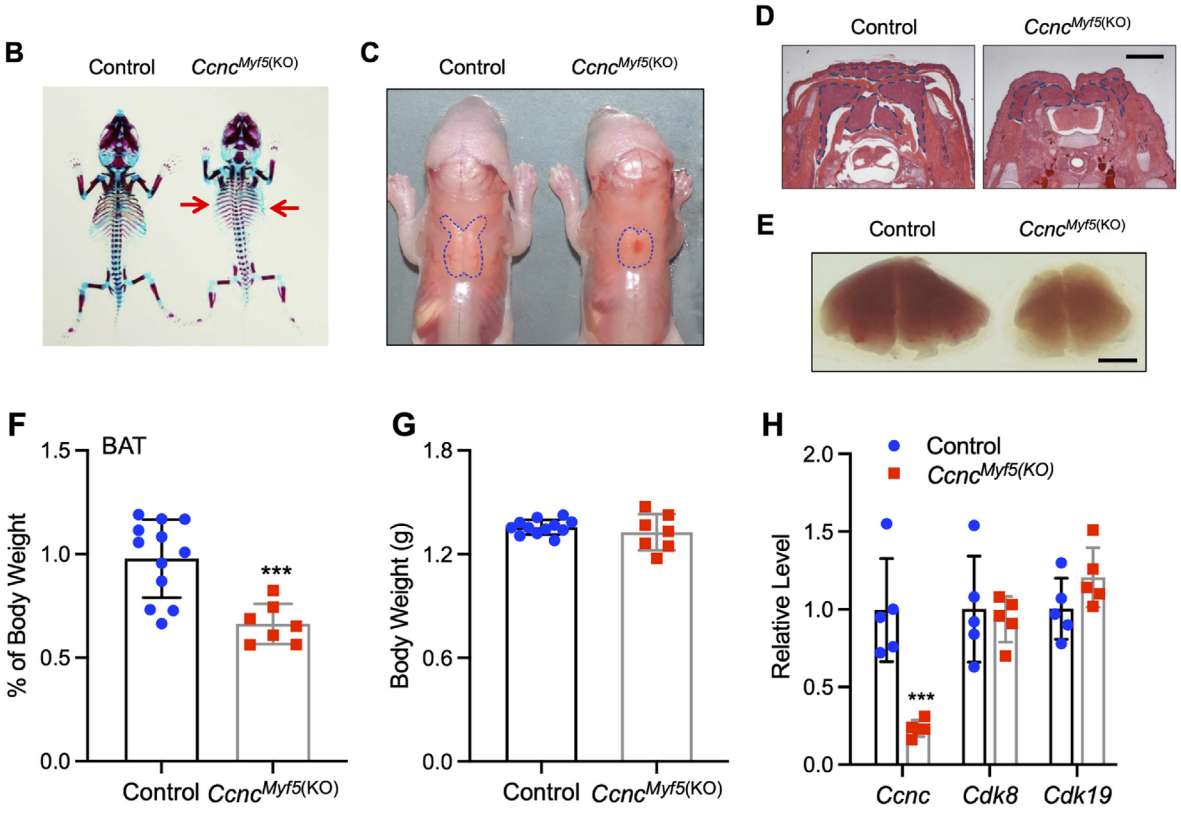

Figure 1: CCNC deficiency in the *Myf5*$^{+}$ lineage causes partial neonatal lethality and prenatal brown fat paucity. (*A*) Summary of the genotypes of mice at E18.5 and P1 stages. (*B*) Representative pictures of Alcian Blue-Alizarin Red Skeletal Staining of the live control and dead *Ccnc*$^{Myf5(KO)}$ mice at P1. The abnormal ribs are indicated by red arrow. (*C*) Macroscopic examination of BAT of the control and *Ccnc*$^{Myf5(KO)}$ mice at P1. BAT is highlighted by dashed lines. (*D*) H&E staining of cervical transverse sections of the control and *Ccnc*$^{Myf5(KO)}$ mice at E18.5. BAT is highlighted by dashed lines. Scale bar, 200 μm. (*E*) Representative images of BAT isolated from the live control and *Ccnc*$^{Myf5(KO)}$ mice at P1. Scale bar, 1 mm. (*F*) Body weight of the control and *Ccnc*$^{Myf5(KO)}$ mice at P1. (*G*) Percentage of BAT weight over body weight of the control and *Ccnc*$^{Myf5(KO)}$ mice at P1. (*H*) qRT-PCR analysis of *Ccnc*, *Cdk8* and *Cdk19* expression in BAT of the control and *Ccnc*$^{Myf5(KO)}$ mice at E18.5. *** $p < 0.001$ vs control. (For interpretation of the references to color in this figure legend, the reader is referred to the Web version of this article.)

progenitor cells, 2) defects in brown adipogenesis, and/or 3) increased death of differentiated brown adipocytes.

To determine whether CCNC deficiency in *Myf5*$^{+}$ cells may reduce the number of brown fat progenitors, we examined the proliferating cells by Ki67 immunostaining in mouse embryonic BAT at E18.5, when brown progenitor cells are abundant [52]. Although CCNC is not directly involved in cell cycle regulation, it has been reported that CCNC can positively or negatively regulate cell cycle progression in a context-dependent manner [40,53]. Consistent with the previous report [52], approximately 50% of the cells were proliferative in the control embryonic BAT as detected by Ki67 immunostaining (Figure 2A,B). However, the number of Ki67^{+} cells in *Ccnc*$^{Myf5(KO)}$ embryonic BAT was significantly less (Figure 2A). Semi-quantitative analyses showed approximately 25% reduction of Ki67^{+} cells in CCNC-knockout embryonic BAT (Figure 2B). This result suggests that CCNC is required for the proliferation of brown fat progenitors.

To examine whether CCNC deficiency in *Myf5*$^{+}$ cells may increase cell death, we performed TUNEL assays for apoptotic cells. As expected, apoptosis is rare in embryonic BAT and CCNC deficiency did not increase the number of apoptotic cells (Figure 2C,D). Thus, loss of CCNC in BAT does not cause apoptosis in embryonic BAT.

To determine whether CCNC deficiency in *Myf5*$^{+}$ cells may inhibit brown adipogenesis *in vivo*, we examined BAT in embryos at E18.5 and newborns at postnatal day 1 (P1). Consistent with the previous report [54], H&E staining showed that the control BAT at E18.5 mostly consisted of brown preadipocytes without visible lipid droplets, while

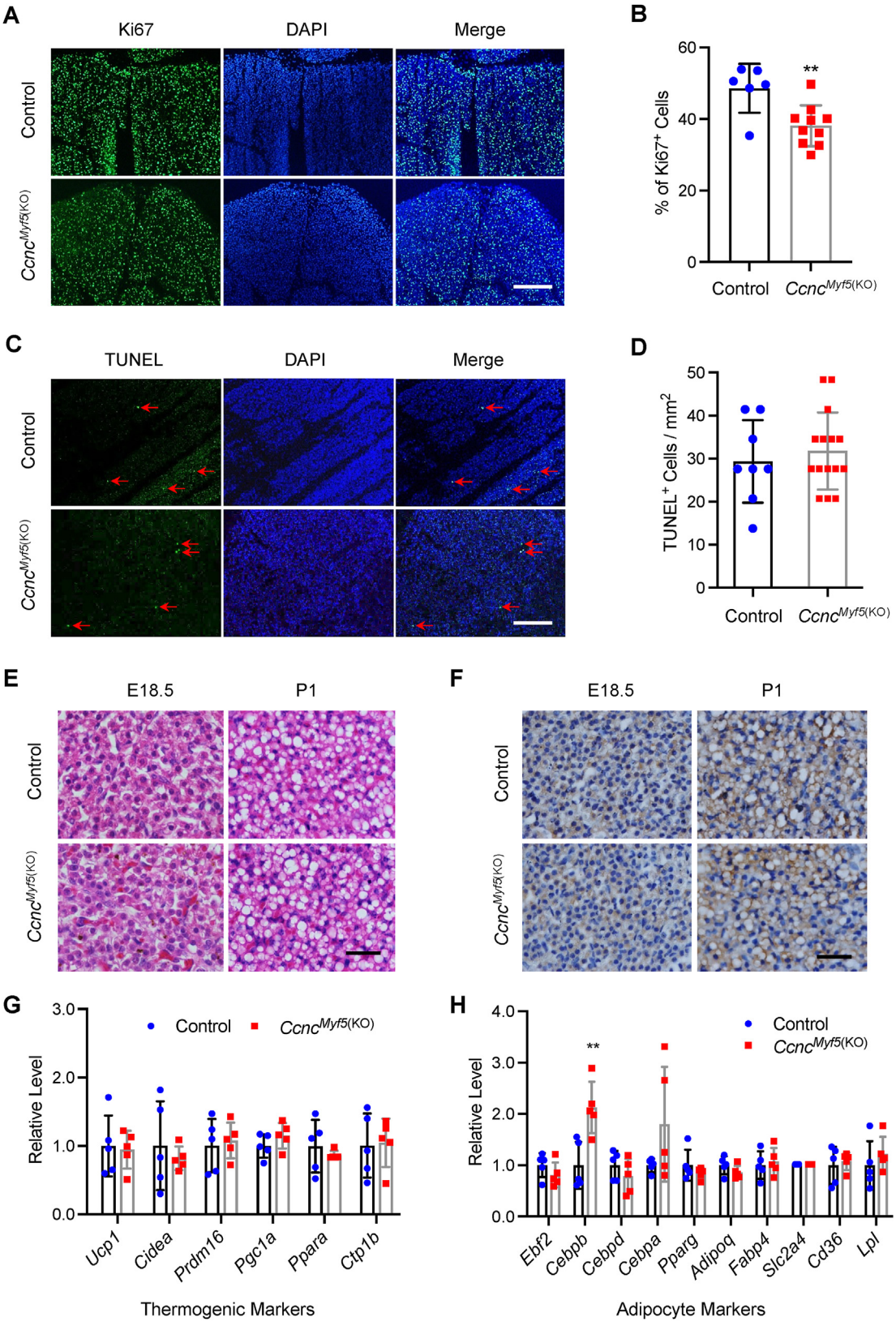

Figure 2: CCNC deficiency in the *Myf5*$^{+}$ lineage inhibits cell proliferation, but not affecting brown adipogenesis and cell death. (*A*) Representative images from Ki67 immunofluorescence on cryosections of BAT from the control and *Ccnc*$^{Myf5(KO)}$ mice at E18.5. Scale bar, 200 μm. (*B*) Quantification of Ki67 positive cells. (*C*) Representative images of TUNEL assays on cryosections of BAT from the control and *Ccnc*$^{Myf5(KO)}$ mice at E18.5. Scale bar, 200 μm. (*D*) Quantification of apoptotic cells. (*E*) H&E staining of paraffin sections of BAT from the control and *Ccnc*$^{Myf5(KO)}$ mice at E18.5 and P1. Scale bar, 30 μm. (*F*) Representative images of UCP1 immunohistochemistry on paraffin sections of BAT from the control and *Ccnc*$^{Myf5(KO)}$ mice at E18.5 and P1. Scale bar, 30 μm. (*G, H*) qRT-PCR analysis of thermogenic genes (*G*) and pan-adipose genes (*H*) in BAT from the control and *Ccnc*$^{Myf5(KO)}$ mice at E18.5. ** $p < 0.01$ vs control. (For interpretation of the references to color in this figure legend, the reader is referred to the Web version of this article.)

the control BAT at P1 was mainly composed of mature brown adipocytes with some lipid droplets (Figure 2E). This is because after birth, brown preadipocytes in BAT rapidly differentiated and become mature brown adipocytes [55]. Previously, we have shown that CCNC deletion in brown preadipocytes completely blocked adipogenesis in tissue culture [43]. To our surprise, BAT of *Ccnc*$^{Myf5(KO)}$ mice showed a similar developmental morphology as control (Figure 2E), indicating that different from tissue culture, CCNC deletion *in vivo* did not inhibit brown adipogenesis. In addition to BAT histology, this conclusion was further supported by analyses of brown fat molecular signatures. As shown in Figure 2F, UCP1 expression in *Ccnc*$^{Myf5(KO)}$ and control mice were indistinguishable at both E18.5 and P1 stages as examined by immunohistochemistry. Consistent with the UCP1 protein levels, qRT-PCR analyses showed that CCNC deficiency did not affect *Ucp1* gene expression (Figure 2G). In fact, the mRNA levels of key thermogenic marker genes, such as *Cidea* and *Prdm16*, and adipocyte marker genes, such as *Pparg*, *Adipoq* and *Fabp4*, were not significantly affected by CCNC deletion, although *Cebpb* was upregulated (Figure 2G,H). These data suggest that CCNC is not essential for brown adipogenesis *in vivo*. Together, these results revealed a cellular mechanism for the reduction of BAT mass in *Ccnc*$^{Myf5(KO)}$ mice, which is the reduction of brown fat progenitor cell proliferation without alteration of adipogenesis or cell death.

3.3. CCNC deficiency impairs lipid accumulation in brown adipocytes

With a limited number of survived *Ccnc*$^{Myf5(KO)}$ mice, we compared with their littermates at the adult stages (around six-month-old) when they were fed with a normal chow diet (NCD). As shown in Figure 3, adult *Ccnc*$^{Myf5(KO)}$ mice were smaller in body size (Figure 3A) and weight (Figure 3B), indicating that CCNC deficiency in the *Myf5*$^{+}$ lineage caused postnatal growth retardation. Consistent with the report that *Myf5*$^{+}$ progenitors are the origin for both brown adipocytes and skeletal muscle cells [10], CCNC was efficiently depleted in both BAT and skeletal muscle of *Ccnc*$^{Myf5(KO)}$ mice (Figure 3C,D). Interestingly, we also detected a small but significant reduction of the *Ccnc* mRNA levels in white fat of *Ccnc*$^{Myf5(KO)}$ mice (Figure 3C), suggesting that some cells in white fat are also originated from *Myf5*$^{+}$ cells. Similar to newborns, adult *Ccnc*$^{Myf5(KO)}$ mice displayed significantly reduced BAT by weight (Figure 3E) or by size (Figure 3F), while skeletal muscles of *Ccnc*$^{Myf5(KO)}$ mice were relatively normal (Figure 3E). Surprisingly, histological analyses revealed that compared to control, CCNC-deficient BAT displayed dramatically less lipid droplets (Figure 3G). Quantitative measurements confirmed that CCNC-deficient BAT had nearly 60% less triglycerides than that of control mice (Figure 3H). Thus, unlike at prenatal and newborn stages, CCNC is critically required for lipid accumulation in BAT of adult mice under the NCD condition.

Since CCNC was deleted in both brown adipocytes and skeletal muscle cells in *Ccnc*$^{Myf5(KO)}$ mice, whether the lipid-poor phenotype of BAT was through cell-autonomous and/or endocrine mechanism(s) requires further investigation. However, the lethality of *Ccnc*$^{Myf5(KO)}$ mice obstructed us from obtaining sufficient mouse samples for further mechanistic studies. Alternatively, to determine whether CCNC regulation of lipid accumulation is cell-autonomous in mature brown adipocytes *in vivo*, we switched to a different mouse model, in which CCNC is deleted specifically in brown adipocyte-specific *Ucp1*$^{+}$ cells by crossing *Ucp1*^{Cre} transgenic mice with *Ccnc*$^{flox/flox}$ mice. Genotyping analyses showed normal Mendelian ratios for all genotypes (data not shown), suggesting that CCNC deletion in *Ucp1*$^{+}$ cells did not cause lethality. The homozygous CCNC knockout (*Ccnc*$^{Ucp1(KO)}$: *Ccnc*$^{flox/flox}$; *Ucp1*^{Cre}) mice were grossly indistinguishable from their littermate controls (data not shown). Similar to *Ccnc*$^{Myf5(KO)}$ mice, *Ccnc*$^{Ucp1(KO)}$ mice had smaller BAT in weight (Figure 3I), while there were no changes in any other organs, including liver, white fat and skeletal muscles (Figure 3J). Real-time qRT-PCR (Figure 3K) and immunoblotting analyses (Figure 3L) confirmed the efficient depletion of CCNC in BAT of *Ccnc*$^{Ucp1(KO)}$ mice. Similar to the *Ccnc*$^{Myf5(KO)}$ mice, the brown fat marker genes, such as *Ucp1*, were unchanged in the *Ccnc*$^{Ucp1(KO)}$ mice (Figure 3M). Interestingly, histological analyses also revealed significantly less lipids in BAT of adult *Ccnc*$^{Ucp1(KO)}$ mice, while the inguinal WAT (iWAT) looked normal (Figure 3N). Thus, CCNC deficiency in the *Ucp1*$^{+}$ lineage does not affect the growth of mice. Collectively, these results suggest that CCNC regulation of lipid accumulation in BAT is likely through cell-autonomous mechanism(s).

3.4. CCNC is required for the expression of key genes mediating *de novo* lipogenesis

To understand how CCNC regulates lipid metabolism in brown adipocytes, we performed RNA sequencing (RNA-seq) analyses. The differential expression data showed that 587 genes were upregulated and 384 genes were downregulated in BAT of *Ccnc*$^{Ucp1(KO)}$ compared to control (*Ccnc*$^{flox/flox}$) mice (Figure 4A), suggesting that CCNC does not have broad transcriptional functions in BAT. Cluster heatmap analyses of differentially expressed genes revealed that the upregulated genes and the downregulated genes belonged to distinct pathways (Figure 4B). Furthermore, the KEGG pathway analyses indicated that the most significantly upregulated pathway was the PPAR signaling pathway (Figure 4C), while the most significantly downregulated pathway was the insulin signaling pathway (Figure 4D). Most relevant to the defects in lipid accumulation was the downregulated pathways, as the insulin signaling pathway is known to play an important role in lipid metabolism of brown fat [17]. Interestingly, the significantly downregulated genes in the insulin signaling pathway included phosphoenolpyruvate carboxykinase (*Pck1*), sterol regulatory element-binding transcription factor-1 *(Srebf1)*, acetyl-CoA carboxylase *(Acaca)* and fatty acid synthase *(Fasn)* (Figure 4E). In fact, the enzymes encoded by *Acaca* and *Fasn* are major components in the DNL (Figure 4F). *Pck1* encodes PEPCK that is a key component of gluconeogenesis in the liver, but in adipocytes PEPCK contributes the backbones for re-esterification of free fatty acids into triglycerides [56] (Figure 4F). Real-time qRT-PCR demonstrated that there was no difference for genes involved in adipogenesis (Figure 4G). Expression of the thermogenic (Figure 4H) and fatty acid oxidation and lipolysis (Figure 4I) programs were also not significantly different between CCNC-deficient BAT and the control BAT. qRT-PCR analyses also validated the RNA-seq data and confirmed that CCNC depletion in brown adipocytes resulted in a significant downregulation of *Pck1* and key lipogenic genes including *Acly*, *Acaca*, and *Fasn* (Figure 5A). A similar downregulation of these genes was also detected in BAT of *Ccnc*$^{Myf5(KO)}$ mice (Figure 5B). Interestingly, CCNC deficiency did not affect the expression of *Gpat*, whose protein product is an important enzyme for triglyceride synthesis (Figure 5B). At the protein level, CCNC deficiency resulted in a robust reduction of FAS and ACC1, but not carnitine palmitoyltransferase 1B (CPT1B), which catalyzes the rate-limiting step of fatty acid oxidation (Figure 5C). Thus, these data suggest that CCNC deficiency in BAT reduces DNL resulting in a decrease of lipid accumulation over time.

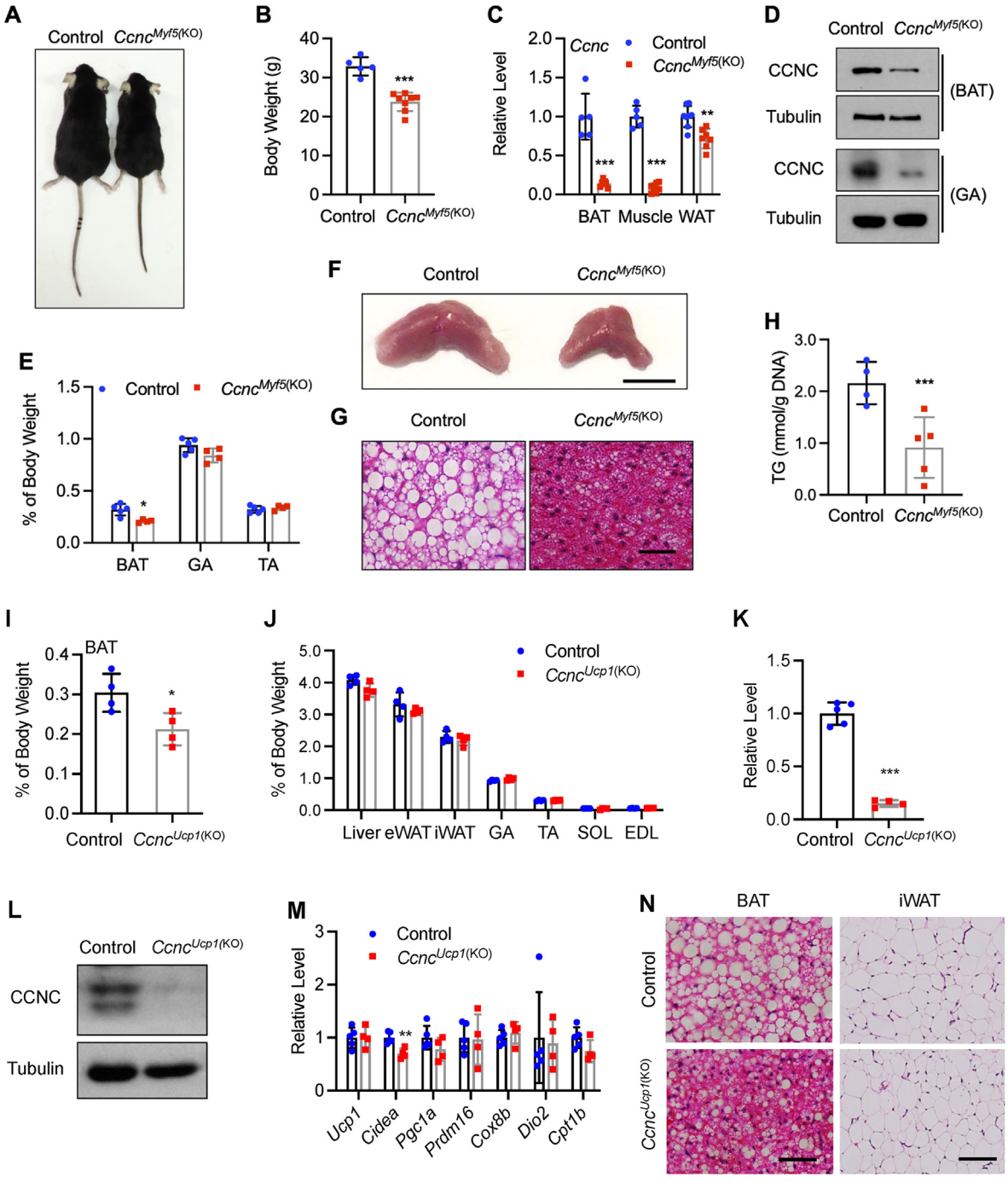

Figure 3: CCNC deficiency reduces lipid accumulation in BAT of adult mice. (*A-H*) $Ccnc^{Myf5(KO)}$ and control mice. (*A*) Representative pictures of mice. (*B*) Body weight. (*C*) qRT-PCR analysis of *Ccnc* expression in BAT, gastrocnemius (GA) muscle and epididymal white adipose tissue (WAT). (*D*) Western blotting analysis of CCNC protein expression in BAT and GA muscle. (*E*) The percentage of BAT, GA muscle and tibialis anterior (TA) muscle weight over body weight. (*F*) Representative macroscopic images of isolated BAT. Scale bar, 0.5 cm. (*G*) H&E staining of paraffin sections of BAT. Scale bar, 50 μm. (*H*) Quantification of triglycerides content in BAT. (*I–M*) $Ccnc^{Ucp1(KO)}$ and control mice. The percentage of BAT (*I*), and liver, epididymal white adipose tissue (eWAT), inguinal white adipose tissue (iWAT), gastrocnemius (GA), tibialis anterior (TA), soleus (SOL) as well as extensor digitorum longus (EDL) muscles (*J*) weight over body weight. *Ccnc* mRNA (*K*) and protein (*L*) levels in BAT. (*M*) qRT-PCR analysis of BAT-related genes. (*N*) H&E staining of BAT and iWAT. Scale bars, 50 μm. All data were from 5 to 7 month-old male mice fed with the normal chow diet. * $p < 0.05$, ** $p < 0.01$, and *** $p < 0.001$ vs control.

3.5. CCNC activates lipogenic gene expression in brown adipocytes through C/EBPα-mediated induction of GLUT4 and ChREBP transcription factors

The expression of key lipogenic genes, such as *Fasn*, is critically activated by two transcription factors SREBP-1 and ChREBP, in response to insulin and carbohydrates, respectively [57,58]. Consistent with our previous discovery that CCNC/CDK8 promotes nuclear/mature SREBP-1 degradation through direct phosphorylation [37], CCNC deficiency caused an increase of nuclear SREBP-1 proteins in BAT (Figure 5C). Although we were unable to exclude the involvement of

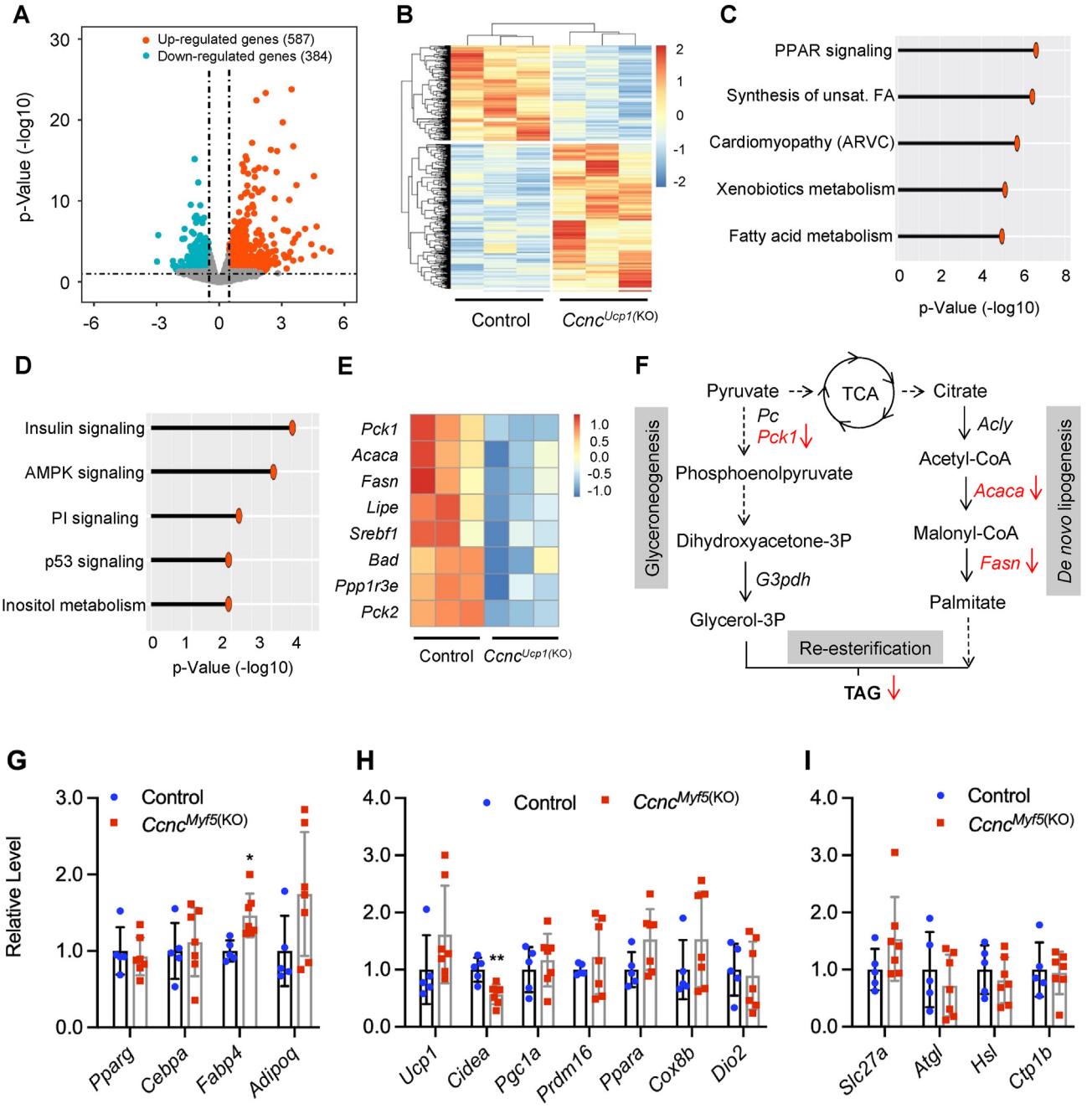

Figure 4: CCNC deficiency impairs lipid synthesis in BAT. *(A)* Volcano plot comparison of gene expression in BAT of $Ccnc^{Ucp1(KO)}$ and control mice (n = 3 per group) by RNA-seq. *(B)* Cluster analysis of all differentially expressed genes in BAT of $Ccnc^{Ucp1(KO)}$ mice. KEGG pathway analyses of signaling pathways up-regulated *(C)* and down-regulated *(D)* in BAT of $Ccnc^{Ucp1(KO)}$ mice. *(E)* Down-regulated genes in insulin signaling pathway are shown in heat map. *(F)* Schematic representation of the effects of CCNC knockout on lipogenic genes expression. Significantly down-regulated genes in this pathway are marked by red color. *Pc*, pyruvate carboxylase; *Gpdh*, Glycerol-3-phosphate dehydrogenase; *Pck1*, Phosphoenolpyruvate carboxykinase 1; *Acly*, ATP-citrate lyase; *Acaca*, Acetyl-CoA carboxylase; *Fasn*, fatty acids synthase. *(G-I)* qRT-PCR analysis of pan-adipose genes *(G)*, BAT-related genes *(H)* and lipid transport and lipolysis genes *(I)* in BAT from control and $Ccnc^{Myf5(KO)}$ mice. * $p < 0.05$ and ** $p < 0.01$ vs control. (For interpretation of the references to color in this figure legend, the reader is referred to the Web version of this article.)

SREBP-1, it is less likely that downregulation of lipogenic genes in CCNC-deficient brown adipocytes is through the SREBP-1 pathway. Interestingly, the *Slc2a4* gene which encode GLUT4, the major glucose transporter in adipose tissues, was significantly downregulated upon CCNC depletion at both mRNA (Figure 5A) and protein (Figure 5C) levels in adult mice. Since adipocyte GLUT4 levels are positively correlated with the ChREBPα transcriptional activity [59], which is activated by glucose metabolites at the posttranslational levels [60,61], we proposed that CCNC regulates lipogenic gene transcription in brown adipocytes through the carbohydrate/GLUT4/ChREBP pathway.

To test this hypothesis, we first studied how CCNC regulates GLUT4 expression. Recently, we have found that CCNC critically supports the transactivation domain (TAD) activity of transcription factor CCAAT/enhancer-binding protein α (C/EBPα) in brown adipocytes [43]. It

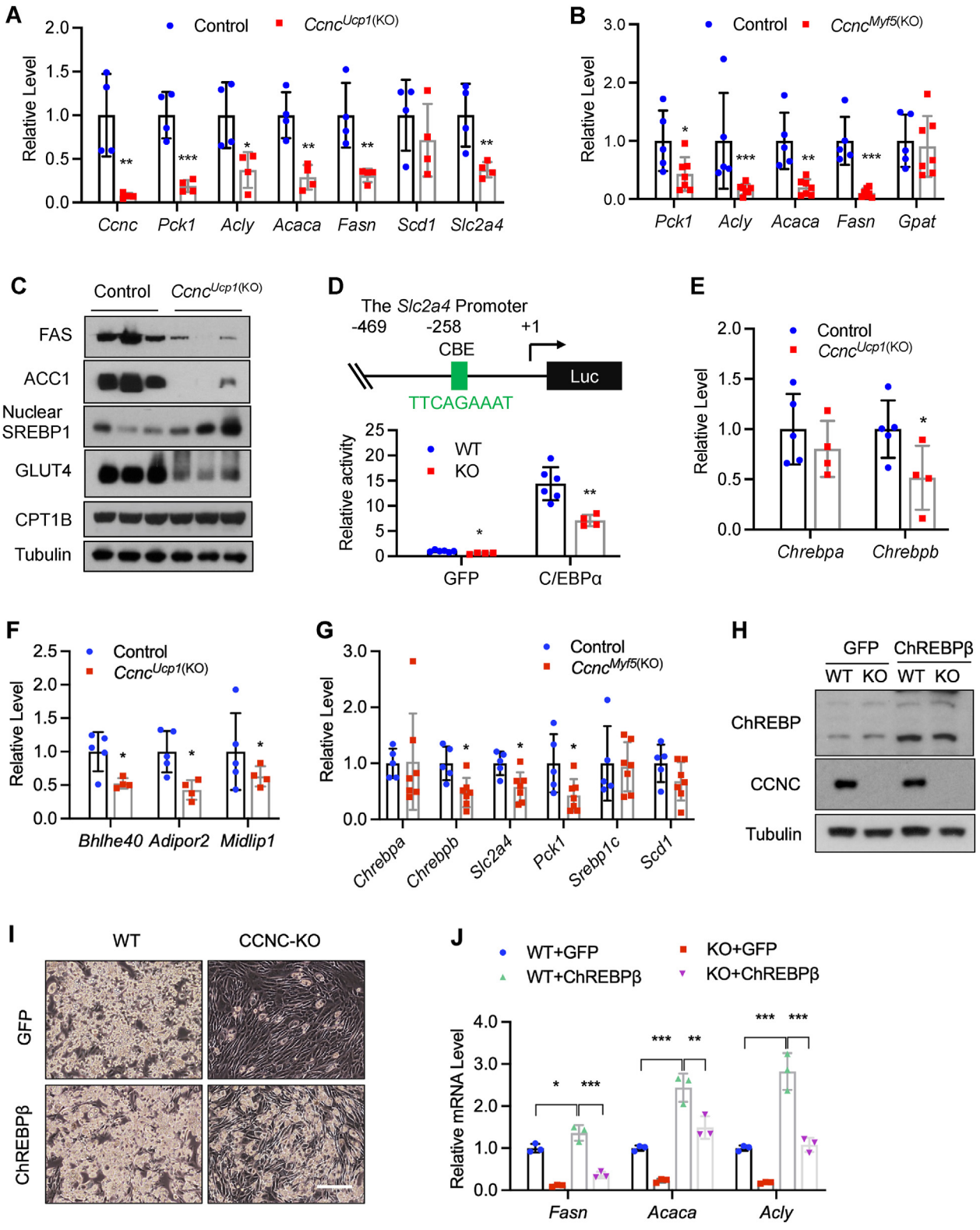

Figure 5: CCNC deficiency inhibits the C/EBPα-GLUT4-ChREBP pathway in BAT. (*A*) qRT-PCR analysis of indicated genes expression in BAT from control and $Ccnc^{Ucp1(KO)}$ mice. (*B*) qRT-PCR analysis of lipogenic genes expression in BAT from control and $Ccnc^{Myf5(KO)}$ mice. (*C*) Western blots analysis of FAS (fatty acid synthase), ACC1 (acetyl-CoA carboxylase-1), Nuclear form of SREBP1 and GLUT4 protein expression in BAT from control and $Ccnc^{Ucp1(KO)}$ mice. (*D*) Dual-luciferase assays of *Glut4* promoter (−469 bp) activity in WT and CCNC−KO brown preadipocytes transfected with GFP or C/EBPα. CRE, C/EBPα responsive-element. qRT-PCR analysis of *Chrebp* (*E*) and its target genes (*F*) expression in BAT from control and $Ccnc^{Ucp1(KO)}$ mice. (*G*) qRT-PCR analysis of indicated genes expression in BAT from control and $Ccnc^{Myf5(KO)}$ mice. (*H*) Western blots analysis of CCNC and overexpressed ChREBPβ in WT and CCNC−KO brown preadipocytes. Overexpressed GFP was used as a transfection control. (*I*) Representative light pictures of differentiated WT and CCNC−KO brown adipocytes with overexpressed GFP or ChREBPβ. Scale bar, 50 μm. (*J*) qRT-PCR analysis of lipogenic genes expression in differentiated WT and CCNC−KO brown adipocytes with overexpressed GFP or ChREBPβ. * $p < 0.05$, ** $p < 0.01$, and *** $p < 0.001$ vs control. (For interpretation of the references to color in this figure legend, the reader is referred to the Web version of this article.)

has been reported that in adipocytes C/EBPα is the key driver for the expression of GLUT4 as well as PEPCK [47,62–64]. There is a C/EBPα-binding element (CBE) in the *Slc2a4* promoter (Figure 5D). To determine whether CCNC deficiency reduces the *Slc2a4* promoter activity, we performed luciferase reporter assays in brown preadipocytes as previously described [43] using a fragment of the *Slc2a4* promoter that contains the CBE motif (Figure 5D). As expected, overexpression of C/EBPα robustly activated the *Slc2a4* promoter in wildtype (WT) cells. However, in CCNC-knockout (KO) cells, C/EBPα was approximately 50% less active on the *Slc2a4* promoter (Figure 5D). This result suggests that CCNC deficiency in brown adipocytes downregulates *Slc2a4* in part due to the reduction of C/EBPα transcriptional activity.

Reduced GLUT4 expression may decrease glucose uptake, thereby suppressing ChREBP activation as well as reducing acetyl-CoA levels. The reduction in ACC1 will also inhibit the formation of malonyl-CoA, a necessary substrate for DNL. ChREBP has two isoforms encoded by *Chrebpa* and *Chrebpb,* and the mRNA levels of *Chrebpb* (encoding ChREBPβ), but not *Chrebp*a (encoding ChREBPα) was significantly decreased in BAT of $Ccnc^{Ucp1(KO)}$ mice (Figure 5E). In addition to lipogenic enzymes and *Chrebpb*, ChREBP target genes also include basic helix-loop-helix family member e40 *(Bhlhe40)*, adiponectin receptor 2 *(Adipor2)* and midline1 interacting protein (*Midlip*) [65]. As shown in Figure 5F, CCNC deficiency downregulated these genes. Consistent with the data from $Ccnc^{Ucp1(KO)}$ mice, BAT from $Ccnc^{Myf5(KO)}$ mice also displayed a reduction of *Chrebpb*, *Slc2a4* and *Pck1*, but not *Chrebpa* and *Srebp1c* (Figure 5G). Thus, these data suggest that CCNC deficiency reduces ChREBP-mediated transcription in brown adipocytes.

The two isoforms of ChREBP transcription factors are differentially regulated at their transcriptional activities. ChREBPα is activated by carbohydrate metabolites, while ChREBPβ is constitutively active due to the lack of the glucose-sensing domain [59]. If CCNC regulation of ChREBP activity is through GLUT4-dependent activation of ChREBPα, overexpression of ChREBPβ should rescue the lipid accumulation defects caused by CCNC deficiency. To this end, we stably overexpressed ChREBPβ in WT and CCNC−KO brown preadipocytes. As shown in Figure 5H, ChREBPβ overexpression was at the similar levels in WT and CCNC−KO cells. We then induced preadipocyte differentiation with an established protocol for eight days. Consistent with our previous report [43], in the control cells in which GFP was overexpressed, CCNC knockout almost completely inhibited lipid accumulation (Figure 5I) and the induction of lipogenic genes such as *Fasn*, *Acaca* and *Acly* (Figure 5J). Overexpression of ChREBPβ enhanced lipid accumulation (Figure 5I) and lipogenic gene expression (Figure 5J) in WT cells. Importantly, overexpression of ChREBPβ was able to partially rescue lipid accumulation (Figure 5I) and lipogenic gene expression (Figure 5J) in CCNC−KO cells. Together, these results suggest that under the NCD condition, ChREBP-mediated transcription is indirectly downregulated in CCNC-deficient brown adipocytes due to reduced C/EBPα activation of GLUT4, causing defects in lipid synthesis.

3.6. HFD feeding eliminates the defect of lipid accumulation in CCNC deficient brown adipocytes

Although hepatocytes in the liver are generally considered as the primary site for DNL and triglyceride synthesis, dietary carbohydrates can also increase the cell-autonomous contribution of *de novo* synthesis to lipid droplets in adipocytes. The NCD in this study is high in carbohydrates (62 kcal%) and low in fat (13 kcal%). Thus, if CCNC regulation of lipid levels in brown adipocytes is through carbohydrate-induced *de novo* lipid synthesis, the lipid-poor phenotype of CCNC-deficient BAT should be eliminated or attenuated when the diet is rich in fat and poor in carbohydrates. To test this hypothesis, we fed $Ccnc^{Ucp1(KO)}$ and control mice with a high-fat diet (HFD) that contains 60 kcal% fat and 20 kcal% carbohydrates. As shown in Figure 6A–E, there was no significant phenotypic difference between $Ccnc^{Ucp1(KO)}$ and control mice in terms of body weight, body mass, GTT, ITT, and histologic features of white fat and liver. Food intake and tissue weight were also not different (Figure S1). However, HFD feeding completely eliminated the NCD-caused difference of lipid levels in BAT between $Ccnc^{Ucp1(KO)}$ and control mice (Figure 6E).

To further study the role of CCNC in regulating adipocyte lipid synthesis, we used another mouse model, in which CCNC was deleted in all adipocytes by crossing $Ccnc^{flox/flox}$ mice with $Adipoq^{Cre}$ transgenic mice ($Ccnc^{Adipoq(KO)}$: $Ccnc^{flox/flox}$; $Adipoq^{Cre}$). The mice were fed with either NCD or HFD. Although CCNC deletion in adipocytes, which was confirmed by qRT-PCR (Figure S2D), did not affect body weight (Figure 6F), but BAT weighed less upon CCNC deletion in $Adipoq^{+}$ cells (Figure 6G). Food intake, fat/lean mass and tissues weight were also not different (Figure S2). Like CCNC deletion in $Ucp1^{+}$ cells, $Ccnc^{Adipoq}$(KO) mice also displayed less lipids in BAT when they were fed with NCD (Figure 6H). Importantly, this phenotype was abolished when the mice were fed with HFD (Figure 6H). There was no histological difference in white fat and liver between CCNC knockout and control mice under both dietary conditions (Figure 6H). Together, our results indicate that CCNC deficiency reduces lipid accumulation in differentiated brown adipocytes only when the diet is rich in carbohydrates, such as NCD. This is consistent with a positive role of CCNC in ChREBP-dependent DNL.

3.7. Brown adipocyte CCNC is not essential for thermoregulation

Under NCD, $Ccnc^{Ucp1(KO)}$ and control mice were similar in terms of body weight (Figure S3A) and food intake (Figure S3B). It has known that BAT plays an important role in glucose homeostasis [66]. To examine whether CCNC in brown adipocytes is involved in the regulation of whole-body glucose metabolism and insulin sensitivity, we performed intraperitoneal glucose- and insulin-tolerance tests (IP-GTT and IP-ITT, respectively). As shown in Figures S3C and S3D, CCNC deficiency in brown adipocytes did not change glucose and insulin tolerance. Moreover, we compared energy metabolism and activities of $Ccnc^{Ucp1(KO)}$ mice with control using a comprehensive laboratory animal monitoring system. As shown in Figures S3E-S3H, there is no difference between $Ccnc^{Ucp1(KO)}$ and control mice in terms of oxygen consumption, carbon dioxide release, respiratory exchange ratio (RER) and heat production, suggesting that CCNC in BAT is not essential for the regulation of basal energy metabolism. Furthermore, CCNC deficiency did not change spontaneous locomotor activities (Figures S3I and S3J). Thus, these data indicate that CCNC in brown adipocytes is not essential for global glucose and energy homeostasis in mice.

Since BAT is important in adaptive non-shivering thermogenesis [67], we then examined the effect of CCNC deletion on body temperature when mice were housed at 6 °C. As expected, body temperature was initially decreased upon acute cold exposure and recovered to normal after chronic cold exposure (Figure 7A). Although the lipid levels in BAT were different (Figure 3N), $Ccnc^{Ucp1(KO)}$ and control mice responded similarly to cold exposure in the first several hours (Figure 7A). Interestingly, after chronic cold exposure $Ccnc^{Ucp1(KO)}$ mice displayed significantly higher body temperatures than control (Figure 7A). Under cold exposure, CCNC deletion did not affect food intake, body weight, and fat/lean mass (Figure 7B–E). While BAT remained smaller in $Ccnc^{Ucp1(KO)}$ mice (Figure 7F), cold exposure did not cause any difference in liver, white fat and skeletal muscle weight (Figure 7G).

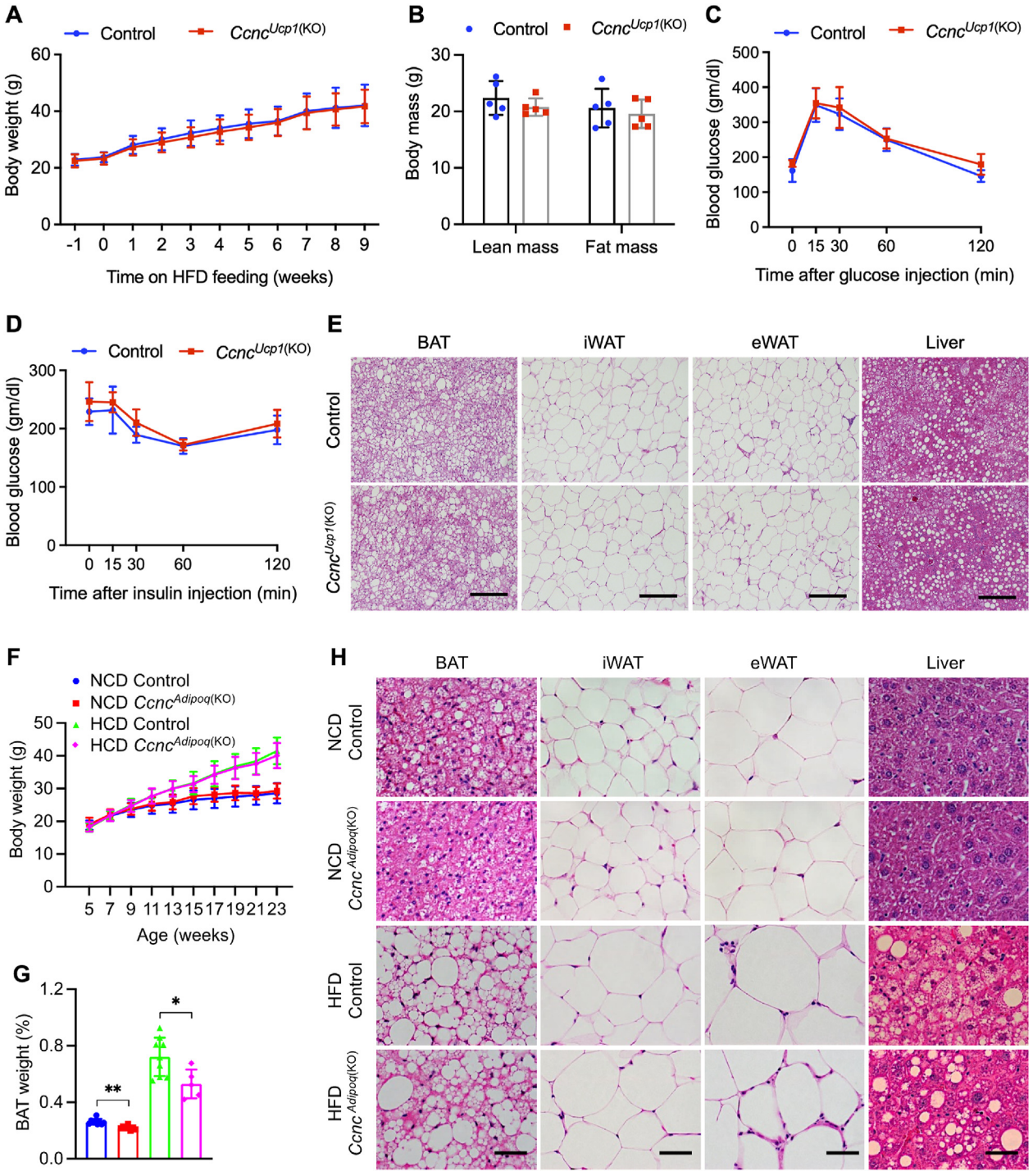

Figure 6: High-fat diet (HFD) feeding eliminates CCNC deficiency-caused defects in BAT lipid accumulation. (*A-E*) From $Ccnc^{Ucp1(KO)}$ and control mice, and (*F–H*) from $Ccnc^{Adipoq(KO)}$ and control mice. (*A*) Body weight of the control (n = 5) and $Ccnc^{Ucp1(KO)}$ (n = 5) mice under HFD. (*B*) Body mass of the control (n = 5) and $Ccnc^{Ucp1(KO)}$ (n = 5) mice on HFD for 12 weeks. (*C*) Blood glucose concentrations during glucose tolerance test (GTT) performed on control and $Ccnc^{Ucp1(KO)}$ mice on HFD for 10 weeks (n = 5 per group). (*D*) Blood glucose concentrations during insulin tolerance test (ITT) performed on control and $Ccnc^{Ucp1(KO)}$ mice on HFD for 14 weeks (n = 5 per group). (*E*) Representative H&E images of BAT, iWAT, eWAT and liver of the control and $Ccnc^{Ucp1(KO)}$ mice under HFD. Scale bars, 50 μm. (*F*) Body weight of the control (n = 8–9) and $Ccnc^{Adipoq(KO)}$ (n = 5–7) mice under chow and HFD. (*G*) BAT weight over body weight of the control (n = 6–8) and $Ccnc^{Adipoq(KO)}$ (n = 5–7) mice under chow and HFD for 24 weeks. (*H*) Representative H&E images of BAT, iWAT, eWAT and liver of the control and $Ccnc^{Adipoq(KO)}$ mice under NCD and HFD. Scale bars, 100 μm * $p < 0.05$, and ** $p < 0.01$ vs control.

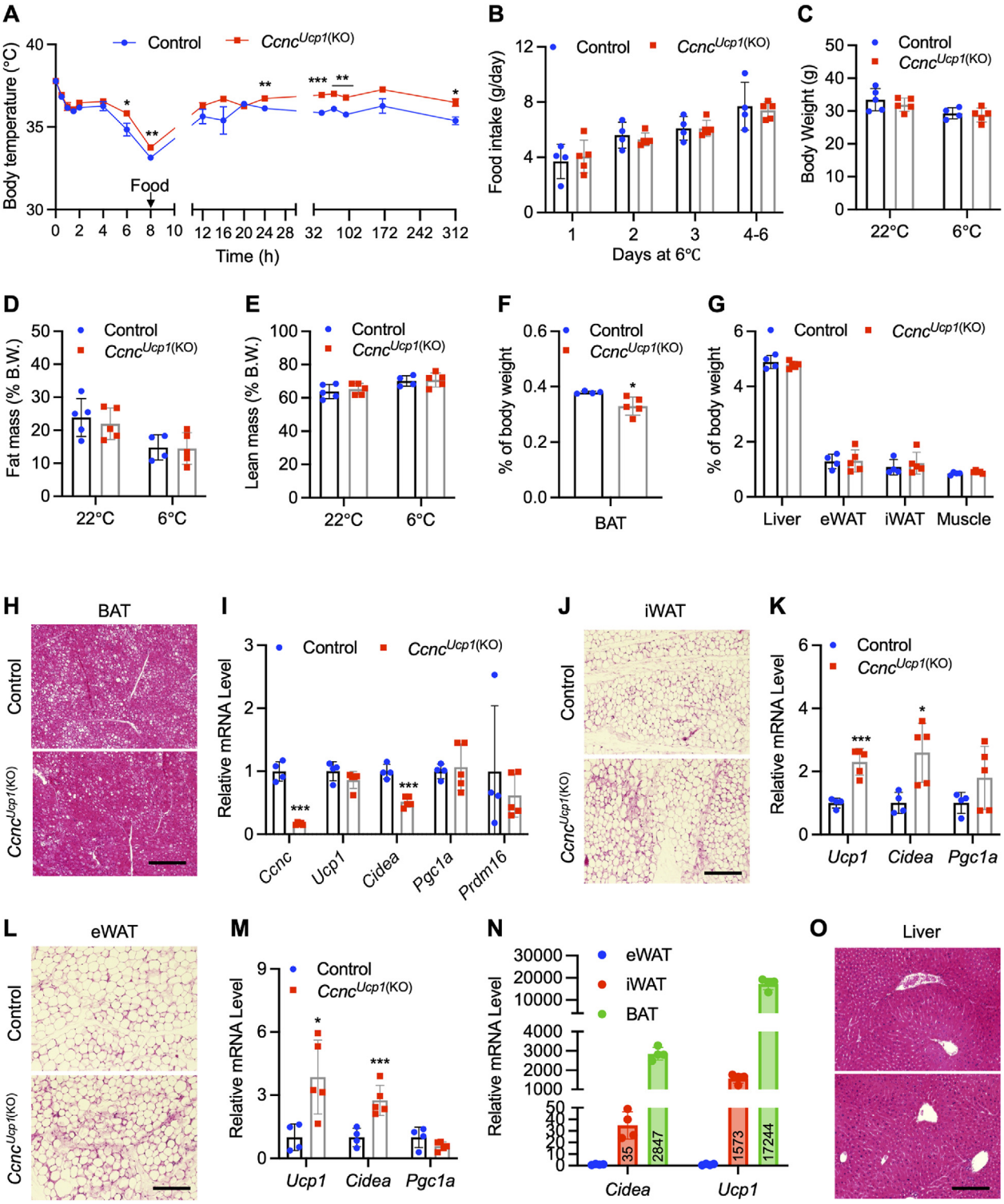

Figure 7: CCNC deficiency in the *Ucp1*$^{+}$ lineage increases body temperature and WAT beiging upon chronic cold exposure. (*A*) Intrarectal temperatures of the 8-month-old control (n = 4) and *Ccnc*$^{Ucp1(KO)}$ (n = 5) mice after the indicated time of housing at 6 °C. (*B*) Average daily food intake of the control (n = 4) and *Ccnc*$^{Ucp1(KO)}$ (n = 5) mice in indicated days at 6 °C. (*C-E*) Body weight, fat mass and lean mass of the control (n = 4–5) and *Ccnc*$^{Ucp1(KO)}$ (n = 5) mice at 22 °C and 6 °C, respectively. (*F, G*) Weight of the indicated tissues of the control (n = 4) and *Ccnc*$^{Ucp1(KO)}$ (n = 5) mice at 6 °C. (*H, J, L, O*) Representative H&E images of BAT, iWAT, eWAT and liver, respectively. (*I, K, M*) Real-time RT-PCR analysis of the indicated genes in BAT, iWAT and eWAT, respectively. (*N*) Relative mRNA level of the indicated genes in wildtype eWAT, iWAT and BAT after two weeks of cold exposure at 6 °C. * $p < 0.05$, ** $p < 0.01$, and *** $p < 0.001$ vs control.

Moreover, CCNC-deficient BAT also displayed reduced lipids after chronic cold exposure (Figure 7H), and key thermogenic genes such as *Ucp1* were similarly induced by cold in $Ccnc^{Ucp1(KO)}$ and control mice (Figure 7I). Consistent with the higher body temperatures, $Ccnc^{Ucp1(KO)}$ mice displayed more iWAT browning by histological features (Figure 7J) and the upregulation of key thermogenic genes (Figure 7K). Similarly, increased browning also observed in epididymal WAT (eWAT) of $Ccnc^{Ucp1(KO)}$ mice (Figure 7L,M), but the contribution of eWAT was less than that of iWAT based upon an at least 35-fold lower induction of the thermogenic genes in eWAT compared to iWAT (Figure 7N). Finally, cold exposure did not cause any difference in the liver (Figure 7O). Together, although CCNC deletion in $Ucp1^{+}$ cells may not affect most physiological functions including brown fat, it increases body temperature upon chronic cold exposure, likely due to the increase of white fat browning.

4. DISCUSSION

Recently, we have shown that CCNC is required for C/EBPα-dependent transcription in brown preadipocytes by activating the transactivation domain of C/EBPα [43]. PPARγ is the master regulator of adipogenesis [68]. Consistent with the fact that most PPARγ-target genes are also co-activated by C/EBPα [69], CCNC knockout completely inhibited brown adipogenesis *in vitro* [43]. Despite the limitations, the $Myf5^{Cre}$ transgenic mice have been used to study brown adipocyte development. To determine whether CCNC is also required for brown adipogenesis *in vivo*, we deleted CCNC specifically in $Myf5^{+}$ progenitor cells using the $Myf5^{Cre}$ transgenic mice. Although most CCNC-deficient mice died shortly after birth, CCNC deletion in the surviving mice displayed a significant reduction of BAT (Figure 1E,F). However, this is probably not due to the reduction of brown adipogenesis. In fact, the remaining CCNC-deficient brown adipocytes are essentially indistinguishable from control in terms of morphology, UCP1 protein levels and key thermogenic and adipogenic marker gene expression (Figure 2E—H). Coincidently, a similar disparity between *in vitro* and *in vivo* adipogenesis was also observed in the case of C/EBPα deletion [70,71]. In our previous study, we found that CCNC deficiency enhanced PPARγ-dependent transcription in the presence of ligands [43]. Thus, one possibility for the different outcomes of CCNC deletion between *in vitro* and *in vivo* is that sufficient PPARγ ligands *in vivo* may make PPARγ active enough to compensate for the reduced transcriptional activity of C/EBPα.

Since neither reduced adipogenesis nor increased cell death were responsible for the reduction of BAT, defects in brown fat progenitor cells became a possibility. During BAT development, the progenitor cell proliferation is peaked at around E18.5 [52]. By immunostaining analyses of Ki67 in mouse embryos, we found that CCNC deletion reduced the number of $Ki67^{+}$ cells at E18.5 by more than 20% (Figure 2A,B). Thus, CCNC deficiency inhibits BAT development due to the decrease of embryonic brown adipocyte progenitor cells. Although it is unclear about how CCNC regulates brown adipocyte progenitors, a previous study has shown that the BMP7 signaling is critical for brown adipocyte progenitor proliferation [52]. Deletion of Type 1A BMP receptor (*Bmpr1a*), a key component of the BMP signaling pathway, in *Myf5*-positive lineage leads to BAT paucity due to impaired progenitor cell proliferation [52]. Moreover, BMPR1a-deficient mice display growth retardation throughout life [52]. These phenotypes are similar to what we have observed in CCNC-deficient mice. Furthermore, CCNC and CDK8 have been reported in cancer cells to regulate the transcriptional activation and turnover of SMAD transcription factors, which are the downstream effectors of the BMP signaling [72]. Therefore, CCNC may regulate brown adipocyte progenitor cell proliferation by activating the BMP signaling pathway.

As the $Ccnc^{Myf5(KO)}$ mice have CCNC deficiency in both brown adipocyte and skeletal muscle progenitor cells, it is also possible that there are alternations in the intercellular crosstalk between these two tissues. For example, skeletal muscle myokines (i.e., irisin) have been reported to induce white adipose tissue browning [73] and BAT controls skeletal muscle function via the secretion of myostatin [74]. Although we cannot as yet exclude tissue-crosstalk as part of the reduction in BAT mass, this cannot account for the reduction in DNL or triglyceride accumulation in the CCNC-deficient BAT as these phenotypes were recapitulated in $Ccnc^{Ucp1(KO)}$ (Figure 3N) or $Ccnc^{Adipoq(KO)}$ (Figure 6H) mice. Reduced lipid accumulation in BAT could be due to decreased lipid transport, decreased lipid synthesis, or increased lipid breakdown and oxidation. RNA-seq analyses of BAT revealed that CCNC deficiency reduced the expression of key enzymes for lipid biosynthesis, including *Fasn*. Although we are unable to exclude the contribution of other mechanisms, the gene expression profiles suggest that decreased lipid biosynthesis is the major cause of reduced lipid accumulation. NCD is rich in carbohydrates, which can serve as the substrates for lipid biosynthesis. Although liver is considered as the major location for DNL, our data suggest that when dietary carbohydrates are abundant, DNL in brown adipocytes is the major contributor to lipid accumulation. Consistent with this model, HFD feeding completely abolished the lipid accumulation defect in two models of CCNC knockout mice. Thus, CCNC is critical for *de novo* lipid synthesis in BAT.

CCNC apparently has an opposite role on lipid synthesis between brown adipocytes and hepatocytes. Previously we have shown that CCNC depletion in hepatocytes promotes lipid accumulation due to increased lipogenesis through upregulation of nuclear SREBP-1 proteins and its target lipogenic genes expression [37]. Consistent with the negative regulation of CCNC/CDK8 on nuclear SREBP-1 proteins [37], CCNC knockout in BAT increased nuclear SREBP-1 protein levels (Figure 5C). However, since SREBP-1 target genes are downregulated in CCNC-deficient BAT, CCNC regulates lipogenic gene expression likely through other transcription factors. As CCNC is an important component of the Mediator kinase module and the Mediator complex functions as a transcription cofactor in a cell and/or context specific manner [75—77], it is likely that the differences between hepatocytes and brown adipocytes is due to the different context role of the CCNC-deficient Mediator complex. For example, CDK8 can serve as both a positive and a negative regulator in transcription through multiple mechanisms such as regulation of transcription factor turnover, of CTD phosphorylation and modulation of activator or repressor functions [78]. On the other hand, although CCNC is classically considered as a part of the Mediator complex in regulating gene transcription, recent studies have also found non-transcriptional mechanisms that are independent of CDK8 or the Mediator, in the regulation of mitochondrial dynamics [79].

In any case, previous studies have shown that in terms of DNL in adipocytes, SREBP-1 may be less important [80—82], while the ChREBP transcription factors play more significant roles [17,59,83]. In fact, most genes in the lipid biosynthesis pathway are activated by both SREBP-1 and ChREBP [84], and the latter includes two isoforms, ChREBPα and ChREBPβ [59]. ChREBPα is ubiquitously expressed and is regulated at the posttranslational levels, while ChREBPβ is constitutively active and is activated by ChREBPs [59]. Although the mechanisms for carbohydrate-induced ChREBPα activation are not fully understood, activated ChREBPα is in complex with MLX to stimulate

the expression of genes primarily involved in glycolysis, DNL, and fatty acid desaturation [85,86]. In this study, we found that many ChREBP target genes including *Chrebpb* are downregulated in CCNC-deficient BAT, suggesting that ChREBP-mediated transcription is reduced. Since glucose flux is a major activator for ChREBPα, we speculate that glucose uptake may be decreased in CCNC-deficient BAT like in previous studies [17,87]. In adipose tissues, there are two major glucose transporters, GLUT1 and GLUT4, that are responsible for transport of glucose across the plasma membranes of adipocytes [88,89]. While GLUT1 functions to maintain the low level of basal glucose uptake, GLUT4 is responsible for insulin-stimulated glucose uptake. Importantly, it has been reported that the GLUT4 level is positively correlated with glucose flux, ChREBPβ and lipogenic gene expression [59,90]. Interestingly, we found that the GLUT4 level is significantly reduced in CCNC-deficient BAT (Figure 5C). Thus, the impaired lipogenic gene expression and lipid accumulation in CCNC-deficient BAT may be due to the downregulation of GLUT4. To understand how CCNC regulates GLUT4 in BAT, we analyzed the promoter of *Slc2a4*, and identified a C/EBPα-binding element. Previous studies have shown that C/EBPα can directly activate GLUT4 expression in adipocytes [47,62–64]. Given our previous study showing that CCNC is critically required for C/EBPα-mediated transcription, it is possible that CCNC regulates GLUT4 expression through C/EBPα. The promoter activity analyses confirmed that CCNC deficiency significantly reduced C/EBPα-induced expression of *Slc2a4* in brown adipocytes (Figure 5D). Thus, although other mechanisms may be also involved, activation of the C/EBPα/GLUT4/ChREBP pathway is highly dependent on CCNC-Mediator in brown adipocytes. Together, these results demonstrate that CCNC is required for the normal development of brown adipose tissues and lipid metabolism in differentiated brown adipocytes *in vivo* as schematically illustrated in Figure 8.

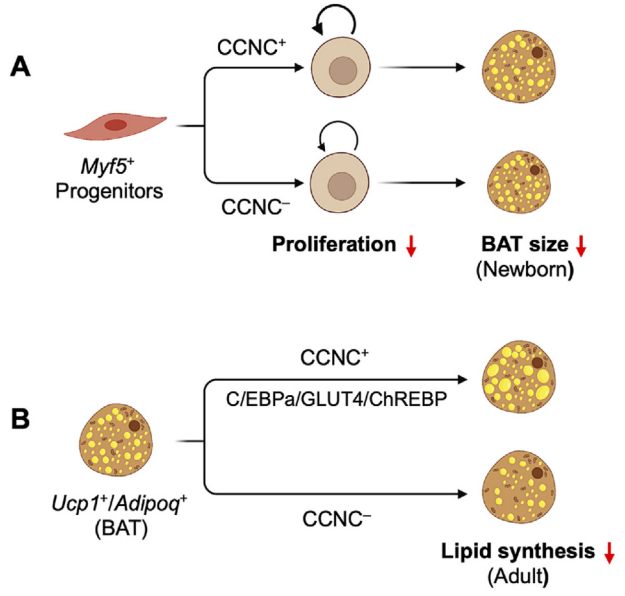

Figure 8: A model depicting the role of CCNC in BAT development and function. At embryonic stage (*A*), CCNC deletion in brown adipocyte progenitor cells results in prenatal BAT paucity due to impairment of brown adipocyte progenitor cell proliferation, while at postnatal stage (*B*), CCNC deficiency in mature brown adipocytes leads to reduced lipid accumulation because of the inhibition of C/EBPα-GLUT4-ChREBP -mediated lipid synthesis pathway. Thus, CCNC plays an important role in both BAT development and lipid accumulation in brown adipocytes. (For interpretation of the references to color in this figure legend, the reader is referred to the Web version of this article.)

Functionally, BAT mass is correlated with body weight control and blood glucose disposal in humans, and in mouse models increasing BAT mass by the means of BAT transplantation improves glucose tolerance, increases insulin sensitivity, reduces body weight, and decreases fat mass of recipient mice [91–93]. Although CCNC deletion in *Ucp1*$^{+}$ cells caused a robust reduction of triglycerides in BAT, it did not change body weight, glucose metabolism and acute cold tolerance (Figure 7), suggesting that DNL in brown adipocytes is not essential for maintaining global glucose homeostasis and basal or cold-induced thermogenesis in mice. Consistent with our findings, BAT-specific FASN or AKT2 deficiency caused the expected defects in DNL but maintained normal thermoregulation in response to acute cold challenge [17,94]. Although lipolysis in brown adipocytes has been believed to produce free fatty acids for heat production, recent studies have argued against its role in cold-induced thermogenesis in mice [95,96]. A possible reason is that the shortage of endogenous fatty acids derived from DNL or lipolysis in BAT can be compensated by the uptake of circulating fatty acids mobilized from WAT or cardiac muscle [95; 96]. Thus, the physiological functions of accumulated lipids in brown adipocytes remain unclear. Nevertheless, DNL in BAT may have more profound effects in humans than animals, because lipogenic genes expression in human BAT is positively correlated with *Ucp1* expression and BMI [17,18]. The GWAS Central data indicate that *Ccnc* is significantly associated with BMI in human. Individuals with SNP in a genomic locus containing *Cdk8* have an increased possibility to develop type 2 diabetes [44]. Interestingly, chronic cold exposure increases body temperature when CCNC is deleted in *Ucp1*$^{+}$ cells (Figure 7A). Although the mechanisms are unclear, this is likely due to an increase of WAT browning. Therefore, it is necessary to further study the metabolic role of adipocyte CCNC in the future.

In summary, using three mouse models we have shown that CCNC in BAT plays different roles at different developmental stages. In the early developmental stages, CCNC controls the prenatal BAT growth; while in adults, CCNC critically regulates lipogenesis in brown adipocytes. These data highlight new functions of CCNC in BAT and provide insights into the molecular regulation of brown fat development and lipid biosynthesis, which may have important implications in developing drugs to target BAT to fight against obesity and its related disorders.

AUTHOR CONTRIBUTIONS

Z.S. and A.M.X. designed and performed the experiments, analyzed and interpreted the data, and wrote the manuscript. Y.L. and G.S. participated in the experiments. T.W. analyzed the RNA-seq data. R.S. generated CCNC-flox mice. J.E.*P. and* F.Y. participated in data interpretation and manuscript writing. F.Y. conceived and supervised this study.

ACKNOWLEDGMENTS

This work was supported by grants from the National Institutes of Health (P30 DK020541 and DK098439, DK117417 and DK110063) and grants from Natural Science Foundation of Guangxi Province (2020GXNSFAA297043) and the Youth Science Foundation of National Natural Science Foundation of China (82100913).

ABBREVIATIONS

CCNC	cyclin C
CDK8	cyclin-dependent kinase 8
SREBP	sterol regulatory element binding protein
ChREBP	carbohydrate response element binding protein

C/EBP	CCAAT/enhancer binding protein
BAT	brown adipose tissue
DNL	*de novo* lipogenesis
NCD	normal chow diet
HFD	high-fat diet.

CONFLICT OF INTEREST

None declared.

APPENDIX A. SUPPLEMENTARY DATA

Supplementary data to this article can be found online at https://doi.org/10.1016/j.molmet.2022.101548.

REFERENCES

[1] Seale, P., Lazar, M.A., 2009. Brown fat in humans: turning up the heat on obesity. Diabetes 58:1482–1484.

[2] Shamsi, F., Wang, C.H., Tseng, Y.H., 2021. The evolving view of thermogenic adipocytes - ontogeny, niche and function. Nature Reviews Endocrinology 17: 726–744.

[3] Cohen, P., Kajimura, S., 2021. The cellular and functional complexity of thermogenic fat. Nature Reviews Molecular Cell Biology 22:393–409.

[4] Lean, M.E., James, W.P., Jennings, G., Trayhurn, P., 1986. Brown adipose tissue uncoupling protein content in human infants, children and adults. Clinical Science 71:291–297.

[5] Cypess, A.M., Lehman, S., Williams, G., Tal, I., Rodman, D., Goldfine, A.B., et al., 2009. Identification and importance of brown adipose tissue in adult humans. New England Journal of Medicine 360:1509–1517.

[6] Virtanen, K.A., Lidell, M.E., Orava, J., Heglind, M., Westergren, R., Niemi, T., et al., 2009. Functional brown adipose tissue in healthy adults. New England Journal of Medicine 360:1518–1525.

[7] van Marken Lichtenbelt, W.D., Vanhommerig, J.W., Smulders, N.M., Drossaerts, J.M., Kemerink, G.J., Bouvy, N.D., et al., 2009. Cold-activated brown adipose tissue in healthy men. New England Journal of Medicine 360: 1500–1508.

[8] Yoneshiro, T., Aita, S., Matsushita, M., Kayahara, T., Kameya, T., Kawai, Y., et al., 2013. Recruited brown adipose tissue as an antiobesity agent in humans. Journal of Clinical Investigation 123:3404–3408.

[9] Cypess, A.M., Weiner, L.S., Roberts-Toler, C., Franquet Elia, E., Kessler, S.H., Kahn, P.A., et al., 2015. Activation of human brown adipose tissue by a beta3-adrenergic receptor agonist. Cell Metabolism 21:33–38.

[10] Seale, P., Bjork, B., Yang, W., Kajimura, S., Chin, S., Kuang, S., et al., 2008. PRDM16 controls a brown fat/skeletal muscle switch. Nature 454: 961–967.

[11] Seale, P., Kajimura, S., Yang, W., Chin, S., Rohas, L.M., Uldry, M., et al., 2007. Transcriptional control of brown fat determination by PRDM16. Cell Metabolism 6:38–54.

[12] Kajimura, S., Seale, P., Kubota, K., Lunsford, E., Frangioni, J.V., Gygi, S.P., et al., 2009. Initiation of myoblast to brown fat switch by a PRDM16-C/EBP-beta transcriptional complex. Nature 460:1154–1158.

[13] Ohno, H., Shinoda, K., Ohyama, K., Sharp, L.Z., Kajimura, S., 2013. EHMT1 controls brown adipose cell fate and thermogenesis through the PRDM16 complex. Nature 504:163–167.

[14] Tseng, Y.H., Kokkotou, E., Schulz, T.J., Huang, T.L., Winnay, J.N., Taniguchi, C.M., et al., 2008. New role of bone morphogenetic protein 7 in brown adipogenesis and energy expenditure. Nature 454:1000–1004.

[15] Fruhbeck, G., Mendez-Gimenez, L., Fernandez-Formoso, J.A., Fernandez, S., Rodriguez, A., 2014. Regulation of adipocyte lipolysis. Nutrition Research Reviews 27:63–93.

[16] Nielsen, T.S., Jessen, N., Jorgensen, J.O., Moller, N., Lund, S., 2014. Dissecting adipose tissue lipolysis: molecular regulation and implications for metabolic disease. Journal of Molecular Endocrinology 52:R199–R222.

[17] Sanchez-Gurmaches, J., Tang, Y., Jespersen, N.Z., Wallace, M., Martinez Calejman, C., Gujja, S., et al., 2018. Brown fat AKT2 is a cold-induced kinase that stimulates ChREBP-mediated de novo lipogenesis to optimize fuel storage and thermogenesis. Cell Metabolism 27:195–209 e196.

[18] Nascimento, E.B.M., Sparks, L.M., Divoux, A., van Gisbergen, M.W., Broeders, E.P.M., Jorgensen, J.A., et al., 2018. Genetic markers of Brown adipose tissue identity and in vitro Brown adipose tissue activity in humans. Obesity 26:135–140.

[19] Malik, S., Roeder, R.G., 2010. The metazoan Mediator co-activator complex as an integrative hub for transcriptional regulation. Nature Reviews Genetics 11: 761–772.

[20] Taatjes, D.J., 2010. The human Mediator complex: a versatile, genome-wide regulator of transcription. Trends in Biochemical Sciences 35:315–322.

[21] Conaway, R.C., Conaway, J.W., 2011. Origins and activity of the Mediator complex. Seminars in Cell & Developmental Biology 22:729–734.

[22] Allen, B.L., Taatjes, D.J., 2015. The Mediator complex: a central integrator of transcription. Nature Reviews Molecular Cell Biology 16:155–166.

[23] Ge, K., Guermah, M., Yuan, C.X., Ito, M., Wallberg, A.E., Spiegelman, B.M., et al., 2002. Transcription coactivator TRAP220 is required for PPAR gamma 2-stimulated adipogenesis. Nature 417:563–567.

[24] Ge, K., Cho, Y.W., Guo, H., Hong, T.B., Guermah, M., Ito, M., et al., 2008. Alternative mechanisms by which mediator subunit MED1/TRAP220 regulates peroxisome proliferator-activated receptor gamma-stimulated adipogenesis and target gene expression. Molecular and Cellular Biology 28:1081–1091.

[25] Grontved, L., Madsen, M.S., Boergesen, M., Roeder, R.G., Mandrup, S., 2010. MED14 tethers mediator to the N-terminal domain of peroxisome proliferator-activated receptor gamma and is required for full transcriptional activity and adipogenesis. Molecular and Cellular Biology 30:2155–2169.

[26] Dean, J.M., He, A., Tan, M., Wang, J., Lu, D., Razani, B., et al., 2020. MED19 regulates adipogenesis and maintenance of white adipose tissue mass by mediating PPARgamma-dependent gene expression. Cell Reports 33:108228.

[27] Wang, W., Huang, L., Huang, Y., Yin, J.W., Berk, A.J., Friedman, J.M., et al., 2009. Mediator MED23 links insulin signaling to the adipogenesis transcription cascade. Developmental Cell 16:764–771.

[28] Yin, J.W., Liang, Y., Park, J.Y., Chen, D., Yao, X., Xiao, Q., et al., 2012. Mediator MED23 plays opposing roles in directing smooth muscle cell and adipocyte differentiation. Genes & Development 26:2192–2205.

[29] Beadle, E.P., Straub, J.A., Bunnell, B.A., Newman, J.J., 2018. MED31 involved in regulating self-renewal and adipogenesis of human mesenchymal stem cells. Molecular Biology Reports 45:1545–1550.

[30] Iida, S., Chen, W., Nakadai, T., Ohkuma, Y., Roeder, R.G., 2015. PRDM16 enhances nuclear receptor-dependent transcription of the brown fat-specific Ucp1 gene through interactions with Mediator subunit MED1. Genes & Development 29:308–321.

[31] Harms, M.J., Lim, H.W., Ho, Y., Shapira, S.N., Ishibashi, J., Rajakumari, S., et al., 2015. PRDM16 binds MED1 and controls chromatin architecture to determine a brown fat transcriptional program. Genes & Development 29: 298–307.

[32] Ito, K., Schneeberger, M., Gerber, A., Jishage, M., Marchildon, F., Maganti, A.V., et al., 2021. Critical roles of transcriptional coactivator MED1 in the formation and function of mouse adipose tissues. Genes & Development 35:729–748.

[33] Jang, Y., Park, Y.K., Lee, J.E., Wan, D., Tran, N., Gavrilova, O., et al., 2021. MED1 is a lipogenesis coactivator required for postnatal adipose expansion. Genes & Development 35:713–728.

[34] Yang, F., Vought, B.W., Satterlee, J.S., Walker, A.K., Jim Sun, Z.Y., Watts, J.L., et al., 2006. An ARC/Mediator subunit required for SREBP control of cholesterol and lipid homeostasis. Nature 442:700–704.

[35] Viscarra, J.A., Wang, Y., Hong, I.H., Sul, H.S., 2017. Transcriptional activation of lipogenesis by insulin requires phosphorylation of MED17 by CK2. Science Signaling 10:eaai8596.
[36] Viscarra, J.A., Wang, Y., Sul, H.S., 2018. MED17 is phosphorylated at S53 by CK2 for transcriptional activation of lipogenic genes in response to insulin. The FASEB Journal 32, 539.6-539.6.
[37] Zhao, X., Feng, D., Wang, Q., Abdulla, A., Xie, X.J., Zhou, J., et al., 2012. Regulation of lipogenesis by cyclin-dependent kinase 8-mediated control of SREBP-1. Journal of Clinical Investigation 122:2417–2427.
[38] Léopold, P., O'Farrell, P.H., 1991. An evolutionarily conserved cyclin homolog from Drosophila rescues yeast deficient in G1 cyclins. Cell 66:1207–1216.
[39] Lew, D.J., Dulic, V., Reed, S.I., 1991. Isolation of three novel human cyclins by rescue of G1 cyclin (Cln) function in yeast. Cell 66:1197–1206.
[40] Li, N., Fassl, A., Chick, J., Inuzuka, H., Li, X., Mansour, M.R., et al., 2014. Cyclin C is a haploinsufficient tumour suppressor. Nature Cell Biology 16: 1080–1091.
[41] Wang, K., Yan, R., Cooper, K.F., Strich, R., 2015. Cyclin C mediates stress-induced mitochondrial fission and apoptosis. Molecular and Cellular Biology 26:1030–1043.
[42] Khakhina, S., Cooper, K.F., Strich, R., 2014. Med13p prevents mitochondrial fission and programmed cell death in yeast through nuclear retention of cyclin C. Molecular Biology of the Cell 25:2807–2816.
[43] Song, Z., Xiaoli, A.M., Zhang, Q., Zhang, Y., Yang, E.S.T., Wang, S., et al., 2017. Cyclin C regulates adipogenesis by stimulating transcriptional activity of CCAAT/enhancer-binding protein alpha. Journal of Biological Chemistry 292: 8918–8932.
[44] Elbein, S.C., Das, S.K., Hallman, D.M., Hanis, C.L., Hasstedt, S.J., 2009. Genome-wide linkage and admixture mapping of type 2 diabetes in African American families from the American diabetes association GENNID (Genetics of NIDDM) study cohort. Diabetes 58:268–274.
[45] Zong, H., Wang, C.C., Vaitheesvaran, B., Kurland, I.J., Hong, W., Pessin, J.E., 2011. Enhanced energy expenditure, glucose utilization, and insulin sensitivity in VAMP8 null mice. Diabetes 60(1):30–38.
[46] Ovchinnikov, D., 2009. Alcian blue/alizarin red staining of cartilage and bone in mouse. Cold Spring Harbour Protocols 2009 pdb prot5170.
[47] Kaestner, K.H., Christy, R.J., Lane, M.D., 1990. Mouse insulin-responsive glucose transporter gene: characterization of the gene and trans-activation by the CCAAT/enhancer binding protein. Proceedings of the National Academy of Sciences of the United States of America 87:251–255.
[48] Bal, N.C., Singh, S., Reis, F.C.G., Maurya, S.K., Pani, S., Rowland, L.A., et al., 2017. Both brown adipose tissue and skeletal muscle thermogenesis processes are activated during mild to severe cold adaptation in mice. Journal of Biological Chemistry 292:16616–16625.
[49] Braun, T., Rudnicki, M.A., Arnold, H.H., Jaenisch, R., 1992. Targeted inactivation of the muscle regulatory gene Myf-5 results in abnormal rib development and perinatal death. Cell 71:369–382.
[50] Kaul, A., Koster, M., Neuhaus, H., Braun, T., 2000. Myf-5 revisited: loss of early myotome formation does not lead to a rib phenotype in homozygous Myf-5 mutant mice. Cell 102:17–19.
[51] Haldar, M., Hancock, J.D., Coffin, C.M., Lessnick, S.L., Capecchi, M.R., 2007. A conditional mouse model of synovial sarcoma: insights into a myogenic origin. Cancer Cell 11:375–388.
[52] Schulz, T.J., Huang, P., Huang, T.L., Xue, R., McDougall, L.E., Townsend, K.L., et al., 2013. Brown-fat paucity due to impaired BMP signalling induces compensatory browning of white fat. Nature 495:379–383.
[53] Ren, S., Rollins, B.J., 2004. Cyclin C/cdk3 promotes Rb-dependent G0 exit. Cell 117:239–251.
[54] Hung, C.M., Calejman, C.M., Sanchez-Gurmaches, J., Li, H., Clish, C.B., Hettmer, S., et al., 2014. Rictor/mTORC2 loss in the Myf5 lineage reprograms brown fat metabolism and protects mice against obesity and metabolic disease. Cell Reports 8:256–271.
[55] Symonds, M.E., 2013. Brown adipose tissue growth and development. Scientifica (Cairo) 2013:305763.
[56] Franckhauser, S., Munoz, S., Pujol, A., Casellas, A., Riu, E., Otaegui, P., et al., 2002. Increased fatty acid re-esterification by PEPCK overexpression in adipose tissue leads to obesity without insulin resistance. Diabetes 51:624–630.
[57] Song, Z., Yang, H., Zhou, L., Yang, F., 2019. Glucose-sensing transcription factor MondoA/ChREBP as targets for type 2 diabetes: opportunities and challenges. International Journal of Molecular Sciences 20:5132.
[58] Yellaturu, C.R., Deng, X., Cagen, L.M., Wilcox, H.G., Mansbach, C.M., Siddiqi, S.A., et al., 2009. Insulin enhances post-translational processing of nascent SREBP-1c by promoting its phosphorylation and association with COPII vesicles. Journal of Biological Chemistry 284:7518–7532.
[59] Herman, M.A., Peroni, O.D., Villoria, J., Schon, M.R., Abumrad, N.A., Bluher, M., et al., 2012. A novel ChREBP isoform in adipose tissue regulates systemic glucose metabolism. Nature 484:333–338.
[60] Kabashima, T., Kawaguchi, T., Wadzinski, B.E., Uyeda, K., 2003. Xylulose 5-phosphate mediates glucose-induced lipogenesis by xylulose 5-phosphate-activated protein phosphatase in rat liver. Proceedings of the National Academy of Sciences of the United States of America 100:5107–5112.
[61] Li, M.V., Chen, W., Harmancey, R.N., Nuotio-Antar, A.M., Imamura, M., Saha, P., et al., 2010. Glucose-6-phosphate mediates activation of the carbohydrate responsive binding protein (ChREBP). Biochemical and Biophysical Research Communications 395:395–400.
[62] Park, E.A., Roesler, W.J., Liu, J., Klemm, D.J., Gurney, A.L., Thatcher, J.D., et al., 1990. The role of the CCAAT/enhancer-binding protein in the transcriptional regulation of the gene for phosphoenolpyruvate carboxykinase (GTP). Molecular and Cellular Biology 10:6264–6272.
[63] Cha, H.C., Oak, N.R., Kang, S., Tran, T.A., Kobayashi, S., Chiang, S.H., et al., 2008. Phosphorylation of CCAAT/enhancer-binding protein alpha regulates GLUT4 expression and glucose transport in adipocytes. Journal of Biological Chemistry 283:18002–18011.
[64] Hernandez, R., Teruel, T., Lorenzo, M., 2003. Insulin and dexamethasone induce GLUT4 gene expression in foetal brown adipocytes: synergistic effect through CCAAT/enhancer-binding protein alpha. Biochemical Journal 372:617–624.
[65] Jeong, Y.S., Kim, D., Lee, Y.S., Kim, H.J., Han, J.Y., Im, S.S., et al., 2011. Integrated expression profiling and genome-wide analysis of ChREBP targets reveals the dual role for ChREBP in glucose-regulated gene expression. PLoS One 6:e22544.
[66] van der Lans, A.A., Hoeks, J., Brans, B., Vijgen, G.H., Visser, M.G., Vosselman, M.J., et al., 2013. Cold acclimation recruits human brown fat and increases nonshivering thermogenesis. Journal of Clinical Investigation 123: 3395–3403.
[67] Peirce, V., Vidal-Puig, A., 2013. Regulation of glucose homoeostasis by brown adipose tissue. Lancet Diabetes & Endocrinology 1:353–360.
[68] Lefterova, M.I., Haakonsson, A.K., Lazar, M.A., Mandrup, S., 2014. PPARγ and the global map of adipogenesis and beyond. Trends in Endocrinology and Metabolism: Trends in Endocrinology and Metabolism 25:293–302.
[69] Lefterova, M.I., Zhang, Y., Steger, D.J., Schupp, M., Schug, J., Cristancho, A., et al., 2008. PPARgamma and C/EBP factors orchestrate adipocyte biology via adjacent binding on a genome-wide scale. Genes & Development 22:2941–2952.
[70] Linhart, H.G., Ishimura-Oka, K., DeMayo, F., Kibe, T., Repka, D., Poindexter, B., et al., 2001. C/EBPalpha is required for differentiation of white, but not brown, adipose tissue. Proceedings of the National Academy of Sciences of the United States of America 98:12532–12537.
[71] Lin, F.T., Lane, M.D., 1994. Ccaat/enhancer binding-protein-alpha is sufficient to initiate the 3t3-L1 adipocyte differentiation program. Proceedings of the National Academy of Sciences of the United States of America 91:8757–8761.
[72] Alarcon, C., Zaromytidou, A.I., Xi, Q., Gao, S., Yu, J., Fujisawa, S., et al., 2009. Nuclear CDKs drive Smad transcriptional activation and turnover in BMP and TGF-beta pathways. Cell 139:757–769.

[73] Bostrom, P., Wu, J., Jedrychowski, M.P., Korde, A., Ye, L., Lo, J.C., et al., 2012. A PGC1-alpha-dependent myokine that drives brown-fat-like development of white fat and thermogenesis. Nature 481:463—U472.
[74] Kong, X., Yao, T., Zhou, P., Kazak, L., Tenen, D., Lyubetskaya, A., et al., 2018. Brown adipose tissue controls skeletal muscle function via the secretion of myostatin. Cell Metabolism 28:631—643 e633.
[75] Donner, A.J., Szostek, S., Hoover, J.M., Espinosa, J.M., 2007. CDK8 is a stimulus-specific positive coregulator of p53 target genes. Molecular Cell 27:121—133.
[76] Galbraith, M.D., Donner, A.J., Espinosa, J.M., 2010. CDK8: a positive regulator of transcription. Transcription 1:4—12.
[77] Galbraith, M.D., Allen, M.A., Bensard, C.L., Wang, X., Schwinn, M.K., Qin, B., et al., 2013. HIF1A employs CDK8-mediator to stimulate RNAPII elongation in response to hypoxia. Cell 153:1327—1339.
[78] Nemet, J., Jelicic, B., Rubelj, I., Sopta, M., 2014. The two faces of Cdk8, a positive/negative regulator of transcription. Biochimie 97:22—27.
[79] Strich, R., Cooper, K.F., 2014. The dual role of cyclin C connects stress regulated gene expression to mitochondrial dynamics. Microb Cell 1(10):318—324.
[80] Sekiya, M., Yahagi, N., Matsuzaka, T., Takeuchi, Y., Nakagawa, Y., Takahashi, H., et al., 2007. SREBP-1-independent regulation of lipogenic gene expression in adipocytes. Journal of Lipid Research 48:1581—1591.
[81] Shimomura, I., Hammer, R.E., Richardson, J.A., Ikemoto, S., Bashmakov, Y., Goldstein, J.L., et al., 1998. Insulin resistance and diabetes mellitus in transgenic mice expressing nuclear SREBP-1c in adipose tissue: model for congenital generalized lipodystrophy. Genes & Development 12:3182—3194.
[82] Shimano, H., Shimomura, I., Hammer, R.E., Herz, J., Goldstein, J.L., Brown, M.S., et al., 1997. Elevated levels of SREBP-2 and cholesterol synthesis in livers of mice homozygous for a targeted disruption of the SREBP-1 gene. Journal of Clinical Investigation 100:2115—2124.
[83] Vijayakumar, A., Aryal, P., Wen, J., Syed, I., Vazirani, R.P., Moraes-Vieira, P.M., et al., 2017. Absence of carbohydrate response element binding protein in adipocytes causes systemic insulin resistance and impairs glucose transport. Cell Reports 21:1021—1035.
[84] Linden, A.G., Li, S., Choi, H.Y., Fang, F., Fukasawa, M., Uyeda, K., et al., 2018. Interplay between ChREBP and SREBP-1c coordinates postprandial glycolysis and lipogenesis in livers of mice. The Journal of Lipid Research 59:475—487.
[85] Iizuka, K., Bruick, R.K., Liang, G., Horton, J.D., Uyeda, K., 2004. Deficiency of carbohydrate response element-binding protein (ChREBP) reduces lipogenesis as well as glycolysis. Proceedings of the National Academy of Sciences of the United States of America 101(19):7281—7286.
[86] Stoeckman, A.K., Ma, L., Towle, H.C., 2004. Mlx is the functional heteromeric partner of the carbohydrate response element-binding protein in glucose regulation of lipogenic enzyme genes. Journal of Biological Chemistry 279:15662—15669.
[87] Tang, Y., Wallace, M., Sanchez-Gurmaches, J., Hsiao, W.Y., Li, H., Lee, P.L., et al., 2016. Adipose tissue mTORC2 regulates ChREBP-driven de novo lipogenesis and hepatic glucose metabolism. Nature Communications 7:11365.
[88] Huang, S., Czech, M.P., 2007. The GLUT4 glucose transporter. Cell Metabolism 5:237—252.
[89] Ebeling, P., Koistinen, H.A., Koivisto, V.A., 1998. Insulin-independent glucose transport regulates insulin sensitivity. FEBS Letters 436:301—303.
[90] Gonzalez, J.T., Richardson, J.D., Chowdhury, E.A., Koumanov, F., Holman, G.D., Cooper, S., et al., 2018. Molecular adaptations of adipose tissue to 6 weeks of morning fasting vs. daily breakfast consumption in lean and obese adults. Journal of Physiology 596:609—622.
[91] Stanford, K.I., Middelbeek, R.J., Townsend, K.L., An, D., Nygaard, E.B., Hitchcox, K.M., et al., 2013. Brown adipose tissue regulates glucose homeostasis and insulin sensitivity. Journal of Clinical Investigation 123:215—223.
[92] Liu, X., Zheng, Z., Zhu, X., Meng, M., Li, L., Shen, Y., et al., 2013. Brown adipose tissue transplantation improves whole-body energy metabolism. Cell Research 23:851—854.
[93] Gunawardana, S.C., Piston, D.W., 2012. Reversal of type 1 diabetes in mice by brown adipose tissue transplant. Diabetes 61:674—682.
[94] Guilherme, A., Pedersen, D.J., Henriques, F., Bedard, A.H., Henchey, E., Kelly, M., et al., 2018. Neuronal modulation of brown adipose activity through perturbation of white adipocyte lipogenesis. Molecular Metabolism 16:116—125.
[95] Shin, H.S., Ma, Y.Y., Chanturiya, T., Cao, Q., Wang, Y.L., Kadegowda, A.K.G., et al., 2017. Lipolysis in Brown adipocytes is not essential for cold-induced thermogenesis in mice. Cell Metabolism 26:764—777 e5.
[96] Schreiber, R., Diwoky, C., Schoiswohl, G., Feiler, U., Wongsiriroj, N., Abdellatif, M., et al., 2017. Cold-induced thermogenesis depends on ATGL-mediated lipolysis in cardiac muscle, but not Brown adipose tissue. Cell Metabolism 26:753—763 e7.

